Vector Correlation and Alignment in Chemistry

Edited by

Gabriel G. Balint-Kurti

Marcelo P. de Miranda

Vector Correlation and Alignment in Chemistry

Edited by

Gabriel G. Balint-Kurti

School of Chemistry
University of Bristol
Bristol
BS8 1TS
United Kingdom

and

Marcelo P. de Miranda

School of Chemistry
University of Leeds
Leeds
LS2 9JT
United Kingdom

Suggested Dewey classification: 541.2

ISBN 0-9545289-2-1

Published by

Collaborative Computational Project
on Molecular Quantum Dynamics (CCP6)
Daresbury Laboratory
Daresbury
Warrington
WA4 4AD
United Kingdom

Preface

This booklet was produced in connection with a CCP6 Workshop on "Vector Correlation and Alignment in Chemistry," held at the University of Bristol, England, 24–27 July, 2005.

CCP6 is the Collaborative Computational Project No. 6 of the United Kingdom Engineering and Physical Sciences Research Council (EPSRC). CCP6 focuses on "Molecular Quantum Dynamics," and regularly organises specialist workshops in its areas of interest. Details of this and other activities of CCP6 may be found on the world wide web at URL http://www.ccp6.ac.uk.

The Bristol Workshop brought together leading experimentalists and theoreticians to share ideas and to discuss the latest developments in the field of chemical stereodynamics. Each speaker in the Workshop was invited to prepare a brief review of the topics covered in his or her lecture, with references to their own and related work. These are the articles that are collected here. They should provide a good introduction to the field for those not working on it, as well as a useful update for those more directly involved.

The editors would like to warmly thank all those who attended the Workshop and gave lectures, presented posters, and took part in the lively discussions.

G. G. Balint-Kurti, Bristol
M. P. de Miranda, Leeds
September 2005

Previous booklets in the CCP6 Workshop series

1. M. M. Law, J. M. Hutson and A. Ernesti (editors), *Fitting Molecular Potential Energy Surfaces*, 1993. ISBN 0-9522736-0-8.

2. G. G. Balint-Kurti and M. M. Law (editors), *Photodissociation Dynamics*, 1994. ISBN 0-9522736-1-6.

3. M. S. Child and M. M. Law (editors), *Intramolecular Dynamics in the Frequency and Time Domains*, 1995. ISBN0-9522736-2-4.

4. A. Ernesti, J. M. Hutson and C. F. Roche (editors), *Molecular Collisions in the Atmosphere*, 1995. ISBN0-9522736-3-2.

5. A. Ernesti, J. M. Hutson and N. J. Wright (editors), *Fashioning a Model: Optimization Methods in Chemical Physics*, 1998. ISBN0-9522736-4-0.

6. R. Prosmiti, J. Tennyson and D. C. Clary (editors), *Molecular Quantum States at Dissociation*, 1998. ISBN0-9522736-5-9.

7. M. M. Law, I. A. Atkinson and J. M. Hutson (editors), *Rovibrational Bound States in Polyatomic Molecules*, 1999. ISBN 0-9522736-6-7.

8. S. C. Althorpe, P. Soldán and G. G. Balint-Kurti (editors), *Time-Dependent Quantum Dynamics*, 2001. ISBN 0-9522736-7-5.

9. I. N. Kozin, M. M. Law and J. N. L. Connor (editors), *Wide-Amplitude Rovibrational Bound States in Polyatomic Molecules*, 2002. ISBN 0-9522736-8-3.

10. P. Soldán, M. T. Cvitaŝ, J. M. Hutson and C. S. Adams (editors), *Interactions of Cold Atoms and Molecules*, 2002. ISBN 0-9522736-9-1.

11. A. Miani, J. Tennyson, T. van Mourik (editors), *High Accuracy Potentials for Quantum Dynamics*, 2003. ISBN 0-9545289-0-5.

12. S. C. Althorpe and G. Worth (editors), *Quantum Dynamics at Conical Intersections*, 2004. ISBN 0-9545289-1-3.

13. D. Sokolovski, J. N. L. Connor and S. Sen (editors), *Semiclassical and Other Methods for Understanding Molecular Collisions and Chemical Reactions*, 2005. ISBN 0-9545289-3-X.

G. G. Balint-Kurti and M. P. de Miranda (eds.)
Vector Correlation and Alignment in Chemistry

$Cl + CH_4$ reaction dynamics

Jon P. Camden and Richard N. Zare
Department of Chemistry, Stanford University, Stanford, CA 94305-5080 USA

The reaction of atomic chlorine and methane to form hydrogen chloride and methyl radical is the first step in the photolytic chlorination of methane. This reaction also plays an important role in the chemistry of the stratosphere, where it terminates the catalytic destruction of ozone [1]. In addition, $Cl + CH_4$ serves as a prototype atom plus polyatom reaction system. For example, the variety of different vibrational modes of the methane reagent and its well characterized infrared spectroscopy provide a testing ground in which to explore the role that vibrational energy plays in elementary reaction dynamics. As will be described in more detail, various vector correlations provide deep insight into how this reaction occurs.

The $Cl + CH_4$ reaction is slightly endoergic, $\Delta H = 600\,\mathrm{cm}^{-1}$ (0.07 eV) [2], and has an estimated activation barrier of $2760\,\mathrm{cm}^{-1}$ (0.34 eV) [3]. The best estimate of the vibrationally adiabatic ground-state barrier, which is a better predictor of threshold energies neglecting tunneling, is $1370\,\mathrm{cm}^{-1}$ (0.17 eV) [3, 4]. The reaction kinetics [1] have been the subject of many studies, particularly because of the non-Arrhenius dependence on temperature.

Attention is drawn to a recent review by Murray and Orr-Ewing [5] for a compilation of work on the $Cl + CH_4$ reaction before 2004. Since this time, however, several new studies have been completed in the groups of Liu [6–8], Crim [9], Orr-Ewing [10], and Zare [11–13]. In this paper, we focus primarily on the work performed in our laboratory.

Our early studies focused on the reaction of Cl with methane in its ground vibrational state [14–16], hereafter referred to as the ground-state reaction, and with one quantum of antisymmetric stretch excitation [14, 17–19]. The Cl atom is generated by the photolysis of molecular chlorine, which yields mostly chlorine in its ground electronic state, and the HCl and CH_3 products are detected by resonance enhanced multiphoton ionization (REMPI). The ground-state reaction forms internally cold HCl products and the differential cross sections (DCSs) indicate that it proceeds primarily via a rebound mechanism. In this mechanism the HCl/DCl products recoil in the backward direction with respect to the incident Cl atom. A further study of the DCS polarization moments indicates that hydrogen atom transfer occurs late in the transition state. Excitation of the C-H stretching vibration (ν_3) opens several new reaction pathways, leading to

rotationally excited HCl($v = 0$) and vibrationally excited but rotationally cold HCl($v = 1$). The HCl($v = 1$) products are found to be sharply forward scattered and suggest a stripping mechanism that occurs at larger impact parameters. This picture is further supported by measurements using aligned reagents, showing that the reaction occurs with the C-H bond axis aligned perpendicular to the Cl-atom velocity vector. The HCl($v = 0$) products are thought to arise from collisions having smaller impact parameters.

The reactivity of spin-orbit excited Cl atom was also examined. We found [20] that its contribution to the total reaction cross section at the energies studied was negligible. More recently, Orr-Ewing and coworkers [10] have examined the reverse reaction, $CH_3 + HCl \rightarrow CH_4 + Cl/Cl^*$, using the photolysis of methyl iodide to generate methyl radicals, and they found a significant production of Cl^*. The two experiments, however, are not strictly related to each other by detailed balance; thus, these findings are not necessarily inconsistent.

We have also examined the effects of overtone excitation on the title reaction, finding strong bond [21, 22] and mode selectivity [13, 22, 23]. For the reaction of Cl with vibrationally excited isotopomers of methane, which are prepared with infrared laser pumping, we find that selective cleavage of either a C-H or C-D bond is possible. The $\nu_3 = 2$ overtone vibration in CH_4, which in the local mode notation is $|1\,1\,0\,0, F_2\rangle$ leads preferentially to stretch excited methyl fragments; thus, the Cl atom reacts with only one local C-H oscillator according to a spectator model. In a related study of the CH_2D_2 isotope, one can excite both the $|1\,1\,0\,0\rangle$ and $|2\,0\,0\,0\rangle$ states; the DCS that results for $|2\,0\,0\,0\rangle$ vibration indicates a wider cone of acceptance than the $|1\,1\,0\,0\rangle$ excitation. Investigation of the $CD_4(\nu_3 = 2)$ isotope reveals similar behavior, but has subtle differences that distinguish it from $CH_4(\nu_3 = 2)$. In summary, a simple spectator model combined with a local mode picture of the methane vibration is found to account well for the observed dynamics and state distributions.

We have also compared the effect of exciting the two nearly isoenergetic stretching fundamentals: the totally symmetric stretch ν_1 and triply degenerate antisymmetric stretch ν_3 [24]. Surprisingly, the measured differential cross sections and state distributions for the two reactions are identical within our experimental uncertainty, suggesting that the mechanism for the two reactions must be quite similar. Measurements of Crim and co-workers [25] indicate the symmetric stretch is more reactive than the antisymmetric stretch, in agreement with theory, but the mechanism for this enhancement is unclear. More work is needed to refine our understanding of this matter.

Our most recent work has focused on the role that bending vibrations play in chemical reactions [11, 12]. The ν_4 vibration is found to enhance the reaction cross section by at least a factor of 2. Furthermore, in the reaction of $Cl + CH_3D(\nu_3 = 1)$, where the predominant motion arises from the three C-H oscillators with little movement by the C-D oscillator, we find no clear bond or mode selectivity. Simple atom plus diatom models are not sufficient to describe

the observed behavior and more work is needed.

We conclude that much progress has been made in understanding the dynamics of the $Cl + CH_4$ reaction, particularly through the measurement of correlated vector properties, but the behavior of this reaction still hold some mysteries that have eluded a simple explanation.

---

[1] H. A. Michelsen, Acc. Chem. Res. **34**, 331 (2001).
[2] R. Atkinson, D. L. Baulch, R. A. Cox, J. R. F. Hampson, J. A. Kerr and J. Troe, J. Phys. Chem. Ref. Data **21**, 1125 (1992).
[3] Y. Zhao, B. J. Lynch and D. G. Truhlar, J. Phys. Chem. A **108**, 4786 (2004).
[4] J. C. Corchado, D. G. Truhlar and J. Espinosa-Garcia, J. Chem. Phys. **112**, 9375 (2000).
[5] C. Murray and A. J. Orr-Ewing, Int. Rev. Phys. Chem. **23**, 435 (2004).
[6] J. Zhou, J. J. Lin, B. Zhang and K. Liu, J. Phys. Chem. A **108**, 7832 (2004).
[7] B. Zhang and K. Liu, J. Chem. Phys. **122**, 101102 (2005).
[8] J. Zhou, B. Zhang, J. J. Lin and K. Liu, Mol. Phys. **103**, 1757 (2005).
[9] S. Yoon, R. J. Holiday and F. F. Crim, J. Phys. Chem. B **109**, 8388 (2005).
[10] B. Retail, J. K. Pearce, C. Murray and A. J. Orr-Ewing, J. Chem. Phys. **122**, 101101 (2005).
[11] Z. H. Kim, H. A. Bechtel, J. P. Camden and R. N. Zare, J. Chem. Phys. **122**, 084303 (2005).
[12] H. A. Bechtel, J. P. Camden, D. J. A. Brown, R. M. Martin, R. N. Zare and K. Vodopyanov, Angew. Chem., Int. Ed. **44**, 2382 (2005).
[13] H. A. Bechtel, Z. H. Kim, J. P. Camden and R. N. Zare, Mol. Phys. **103**, 1837 (2005).
[14] W. R. Simpson, T. P. Rakitzis, S. A. Kandel, T. Levon, and R. N. Zare, J. Phys. Chem. **100**, 7938 (1996).
[15] T. P. Rakitzis, S. A. Kandel, T. Levon and R. N. Zare, J. Chem. Phys. **107**, 9392 (1997).
[16] S. A. Kandel and R. N. Zare, J. Chem. Phys. **109**, 9719 (1998).
[17] W. R. Simpson, A. J. Orr-Ewing, and R. N. Zare, Chem. Phys. Lett. **212**, 163 (1993).
[18] W. R. Simpson, T. P. Rakitzis, S. A. Kandel, A. J. Orr-Ewing and R. N. Zare, J. Chem. Phys. **103**, 7313 (1995).
[19] A. J. Orr-Ewing, W. R. Simpson, T. P. Rakitzis, S. A. Kandel, and R. N. Zare, J. Chem. Phys. **106**, 5961 (1997).
[20] Z. H. Kim, A. J. Alexander, H. A. Bechtel and R. N. Zare, J. Chem. Phys. **115**, 179 (2001).
[21] Z. H. Kim, H. A. Bechtel and R. N. Zare, J. Am. Chem. Soc. **123**, 12714 (2001).
[22] H. A. Bechtel, Z. H. Kim, J. P. Camden, and R. N. Zare, J. Chem. Phys. **120**, 791 (2004).
[23] Z. H. Kim, H. A. Bechtel and R. N. Zare, J. Chem. Phys. **117**, 3232 (2002).
[24] H. A. Bechtel, J. P. Camden, D. J. A. Brown and R. N. Zare, J. Chem. Phys. **120**, 5096 (2004).

[25] S. Yoon, R. J. Holiday, E. L. Sibert and F. F. Crim, J. Chem. Phys. **119**, 9568 (2003).

G. G. Balint-Kurti and M. P. de Miranda (eds.)
Vector Correlation and Alignment in Chemistry

Orbital alignment in photodissociation: determination of scattering amplitudes and phases beyond the axial recoil approximation

Vladislav V. Kuznetsov[1] and Oleg S. Vasyutinskii[2]

[1] *State University of Aerospace Instrumentation, 190000 St.Petersburg, Russia*
[2] *Ioffe Physico-Technical Institute, Russian Academy of Sciences, 194021 St.Petersburg, Russia*

Photodissociation of molecules is one of the basic processes occurring in nature. In general, treatment of the photodissociation process includes translational anisotropy and angular momentum distribution of photofragment state multipoles [1, 2], described by a set of anisotropy parameters, which can be directly determined from experiment. It has been recently shown [3] that the anisotropy parameters are closely related to the magnitudes and relative phases of the photofragmentation T matrix elements, resulting from ab initio calculations. Comparison of all possible photodissociation scattering amplitudes and phases determined from experiment with their theoretical values meets the condition of the complete experiment [4] and can be used for verification of theoretical models and provides a new powerful tool for investigation of the photodissociation dynamics.

Considering the photodissociation of a diatomic molecule AB which produce fragments A and B, the photofragment state multipoles $\rho_{KQ}(\theta,\phi)$ as function of the recoil angles θ and ϕ in the first order time-dependent perturbation theory can be written as [5]:

$$\begin{aligned}\rho_{KQ}(\theta,\phi) = \frac{3}{4\pi}\left(\frac{2K+1}{2j_A+1}\right)^{1/2} \\ \times \sum_{q,q',Q'}\sum_{k_d,q_d}(-1)^{K+q'}(2k_d+1)^{1/2}\,E_{k_dq_d}(\mathbf{e})\begin{pmatrix}1 & 1 & k_d\\ q' & -q & -Q'\end{pmatrix} \\ \times \frac{f_K(q,q')}{f_0(0,0)+2f_0(1,1)} D^{K}_{QQ'}{}^{*}(\phi,\theta,0)\,D^{k_d}_{q_dQ'}(\phi,\theta,0)\,d^{k_d}_{Q'\,Q'}(\gamma), \qquad (1)\end{aligned}$$

where $E_{k_dq_d}(\mathbf{e})$ is the photon polarization matrix, the product of two D-functions, $D^{K}_{QQ'}{}^{*}(\phi,\theta,0)\,D^{k_d}_{q_dQ'}(\phi,\theta,0)$ represents the *kinematic* part and the dynamical functions $f_K(q,q')$ with their ranks K describe the photodissociation dynamics including coherent effects and nonadiabatic interactions.

Equation (1) describes angular distribution of photofragment state multipoles and takes into consideration possible radial nonadiabatic interaction and rotation of the molecular axis, but not the Coriolis interaction. Summation over the total angular momenta J and J' including the coherent terms $J \neq J'$ has been proceeded in eq. (1). This procedure in fact implies the formation of the *photofragment wave packet* in the molecular excited state and describes the fast photodissociation of a rotating molecule when the individual J states are not resolved.

Equation (1) treats the electronic movement quantum mechanically and the nuclear movement quasiclassically using the quasiclassical approximation which allows to separate the regions of the internuclear distance R where the dissociation dynamics is mostly adiabatic from the relatively narrow regions where the nonadiabatic interactions occur. Within this approximation the scattering matrix $S^J_{\bar{k};\,k}$ can be factorized as:

$$S^J_{\bar{k};\,k} \approx \eta^J_{\bar{k};\,k} e^{-2i\,\delta^J_k}, \tag{2}$$

where k in the outgoing channel, $\bar{k}$ is an incoming channel, J is the total molecular angular momentum, the phase δ^J_k is close to the elastic scattering phase which is assumed to be large and leads to the fast oscillations of the exponent as function of J, while the term $\eta^J_{\bar{k};\,k}$ describes nonadiabatic interactions and weakly depends on J.

The d-function $d^{k_d}_{Q'\,Q'}(\gamma)$ in eq. (1) is the *rotational factor* which depends on the rank of the incident photon polarization matrix k_d, on dissociation mechanism, and on the classical angle of rotation of the molecular axis γ. In the axial recoil approximation, $\gamma = 0$, eq. (1) is equivalent to the expression given by Siebbeles and co-workers [2]. If the Coriolis interaction can be neglected, the dynamical functions for rotating molecules are the same as in the Siebbeles and co-workers theory [2], while the corresponding state multipole recoil distributions can be presented in the same form as in the non-rotating case after multiplying each of the anisotropy parameter by a certain *rotation factor* $d^{k_d}_{Q'\,Q'}(\gamma)$.

Particularly, if $K = 0$, the state multipole $\rho_{00}(\theta, \varphi)$ describes the photofragment angle dependence $N = (2j_A + 1)^{1/2}\rho_{00}(\theta, \varphi)$ and can be presented in the following traditional form:

$$N \;=\; \frac{1}{4\pi}\left[1 + \beta\, P_2(\cos\Theta)\right], \tag{3}$$

where Θ is the angle between the light polarization vector $\mathbf{e}$ and the recoil vector $\mathbf{k}$ and β in eqs. (3) is the zero-rank anisotropy parameter:

$$\beta \;=\; P_2(\cos\gamma)\,\beta^{(0)} \tag{4}$$

where $\beta^{(0)}$ is the anisotropy parameter of the molecule which does not rotate during dissociation. This result is in perfect agreement with the previous results [6].

K	1	2
α_K	$\alpha_1^{(0)} \cos\gamma$	$\alpha_2^{(0)} P_2(\cos\gamma)$
s_K	—	$s_2^{(0)}$
γ_K	$\gamma_1^{(0)} \dfrac{1+\cos\gamma}{2}$	$\gamma_2^{(0)} \dfrac{2\cos^2\gamma+\cos\gamma-1}{2}$
γ'_K	$\gamma'^{(0)}_1 \dfrac{2\cos^2\gamma+\cos\gamma-1}{2}$	$\gamma'^{(0)}_2 \dfrac{1+\cos\gamma}{2}$
η_K	—	$\eta_2^{(0)} \dfrac{(1+\cos\gamma)^2}{4}$

TABLE I: Rotation factors with $K = 1$ or 2.

If $K = 1...4$, each state multipole $\rho_{KQ}(\theta,\varphi) \propto \langle j_Q^{(K)} \rangle$ describes the corresponding photofragment density matrix multipole expansion term [1]. All possible in eq. (1) *rotation factors* are collected in Tables I and II, where the superscript index (0) indicates the anisotropy parameters for non-rotating molecules.

The rotation factors $d^{k_d}_{Q'\,Q'}(\gamma)$ depend on the rank of the dissociation photon polarization matrix k_d, on the index Q' describing coherent and incoherent excitation of the molecule, and on the classical angle of rotation of the molecular axis γ. The γ-dependence of each anisotropy parameter in Tables I and II indicates the mechanism of production of the fragment angular momentum polarization in a corresponding reaction channel. For instance, the anisotropy parameters which are proportional to the *first power* of $\cos\gamma$, relate to the multipole polarization due to the incident photon *helicity*. These dissociation mechanisms can be initiated only with circularly polarized light. The anisotropy parameters which

K	3	4
α_K	$\alpha_3^{(0)} \cos\gamma$	$\alpha_4^{(0)} P_2(\cos\gamma)$
s_K	—	$s_4^{(0)}$
γ_K	$\gamma_3^{(0)} \dfrac{1+\cos\gamma}{2}$	$\gamma_4^{(0)} \dfrac{2\cos^2\gamma+\cos\gamma-1}{2}$
γ'_K	$\gamma'^{(0)}_3 \dfrac{2\cos^2\gamma+\cos\gamma-1}{2}$	$\gamma'^{(0)}_4 \dfrac{1+\cos\gamma}{2}$
η_K	$\eta_3^{(0)} \dfrac{(1+\cos\gamma)^2}{4}$	$\eta_4^{(0)} \dfrac{(1+\cos\gamma)^2}{4}$

TABLE II: Rotation factors with $K = 3$ or 4.

are proportional to the *second power* of $\cos\gamma$ relate to the multipole polarization due to the *alignment* of the light polarization vector **e**. These dissociation mechanisms can be initiated either by linear, or by circular light polarization, or by unpolarized light. It is clear that, in general, rotation of the molecular axis reduces the anisotropy.

---

[1] R. N. Zare, *Angular Momentum*, World Scientific, New York, 1988.
[2] L. D. A. Siebbeles, M. Glass-Maujean, O. S. Vasyutinskii, J. A. Beswick, O. Roncero, J. Chem. Phys. **100**, 3610 (1994).
[3] G. G. Balint-Kurti, A. J. Orr-Ewing, J. A. Beswick, A. Brown, O. S. Vasyutinskii, J. Chem. Phys. **116**, 10760 (2002).
[4] U. Fano and J. H. Macek, Rev. Mod. Phys. **45**, 553 (1973).
[5] V. V. Kuznetsov and O. S. Vasyutinskii, J. Chem. Phys. (2005), in press.
[6] R. J. Gordon and G. E. Hall, Adv. Chem. Phys. **96**, 1 (1996).

G. G. Balint-Kurti and M. P. de Miranda (eds.)
Vector Correlation and Alignment in Chemistry

Pulsed-laser preparation of polarized atoms from molecular photodissociation

Luis Rubio-Lago,[1] Dimitris Sofikitis,[1,2]
Antonis Koubenakis,[1,2] and T. Peter Rakitzis[1,2]

[1]*Institute of Electronic Structure and Laser, Foundation for Research and Technology-Hellas, 71110 Heraklion-Crete, Greece*
[2]*Department of Physics, University of Crete, P. O. 2208, 71003 Voutes-Heraklion, Greece*

Polarized atoms are used to study spin-dependent phenomena in many fields, such as nuclear, atomic, molecular, and surface scattering [1–3], and medical imaging using hyperpolarized noble gases [4]. Atoms and molecules posses, in general, *electronic* (J), *nuclear* (I) and *rotational* angular momentum. These angular momenta can be considered to be independent on timescales much shorter than their coupling timescales, so that one of them can be polarized independently. On longer timescales, this polarization will be transferred to the other angular momenta. We will discuss mechanisms that can polarize *either* J *or* I via molecular excitation and photodissociation. The aim of this paper is to show that the appropriate combination of these two mechanisms can produce highly polarized atoms at high density from the pulsed-laser photodissociation of polarized molecules. We also contrast the advantages and disadvantages with respect to existing techniques.

Spin-polarized atoms were first produced using the Stern-Gerlach separation technique [5, 6], which involves passing an atomic beam through an inhomogeneous magnetic field. This technique remains the most general method for producing polarized atoms, as long as an appropriate atomic beam can be produced. Drawbacks include the complexity of the experimental setup, the limited atomic beam density (of about 10^{15} atoms/s in favorable cases), and the poor time-resolution.

Optical pumping [7] is a very powerful technique, and variants of optical pumping are used in various fields of modern atomic physics, such as laser cooling, Bose-Einstein condensation, and the production of spin polarized atoms. For example, circular polarized light ($\sigma(+)$ excitation in this case) pumps the $m = -1/2$ ground state of Rubidium to the $m = +1/2$ excited state, whereas the $m = +1/2$ ground state cannot be pumped as there is no $m = +3/2$ excited state. Collisional quenching transfers population back to both ground spin states. The $m = +1/2$ state has no significant losses, whereas it has significant gains from

excited state quenching; therefore, after several absorption cycles, nearly 100% of the population is transferred to the $m = +1/2$ state. The hyperfine interaction transfers polarization to the nuclear spin, so that, after additional pumping, the nuclear spin is also polarized. The success of optical pumping hinges on a large pumping rate (compared to the depolarization rate). Optical pumping has proved extremely successful for the alkali atoms, which have very strong appropriate transitions [7] (with absorption cross sections $\sigma_{\rm abs} \approx 10^{-10}\,{\rm cm}^2$) in the visible where powerful cw laser sources are readily available. However, most other atoms do not have strong ground-state absorptions where powerful cw sources are currently available, and thus optical pumping has been limited to mostly the alkali atoms. Recently, a very weak cw source at Lyman-α was produced which may allow laser cooling of hydrogen atoms [8]. Improvements in this direction may make optical pumping applicable to other atoms. A further extension of the optical pumping technique is spin-exchange optical pumping (SEOP) [2, 9, 10]. Noble gases with non-zero nuclear spin (*e.g.*, ^{3}He and ^{129}Xe) are mixed with alkali atoms as they are optically pumped. For example, Rubidium electronic spin-polarization is transferred to the ^{3}He nuclear spin via collisions:

$$\mathrm{Rb}(\uparrow e) + {}^3\mathrm{He}(\downarrow n) \rightarrow \mathrm{Rb}(\downarrow e) + {}^3\mathrm{He}(\uparrow n). \tag{1}$$

Using this technique, several atmospheres of ^{3}He can be polarized to $P = 70\%$ over several hours of SEOP.

A method for producing high-density polarized atoms from the photodissociation of diatomic molecules was proposed by van Brunt and Zare in 1968 [11], which exploits the fact that the projection of electronic angular momentum, for prompt photodissociation, is conserved within the atomic photofragments. In fact, the electronic states of diatomic molecules correlate adiabatically, at large internuclear separation, to atoms in specific $|JM\rangle$ states:

$$\mathrm{AB}(\Omega_i) \xrightarrow{R\rightarrow\infty} \mathrm{A}(J_\mathrm{A}, M_\mathrm{A}) + \mathrm{B}(J_\mathrm{B}, M_\mathrm{B}) \tag{2}$$

where AB is a diatomic molecule, Ω_i is the projection of the total electronic angular momentum of electronic state i along the AB bond axis, and $(J_\mathrm{A}, M_\mathrm{A})$ and $(J_\mathrm{B}, M_\mathrm{B})$ are the atomic states of atoms A and B, respectively. Conservation of angular momentum projection along the recoil direction yields the important constraint:

$$\Omega_i = M_\mathrm{A} + M_\mathrm{B}. \tag{3}$$

For optical excitation of a particular Ω_i state, prompt adiabatic dissociation will produce atoms in particular m states.

The strength of the idea is that the mechanism of production of the polarized atoms is a natural physical process (photodissociation) and does not require a

complicated experimental preparation, such as Stern-Gerlach separation. In addition, the density of the polarized atoms can be extremely high, approximately as high as the parent molecule density, which is much higher than that possible with most other techniques. Possible disadvantages include: a) exclusive optical excitation of particular Ω_i states is not always possible, b) dissociation is not necessarily adiabatic, c) even for adiabatic dissociation the photofragment atomic polarization is not necessarily 100% and is often less, d) maximum polarization (in the case of atomic orientation) is achieved only for recoil directions parallel to the quantization axis of the photolysis laser (*i.e.*, the propagation direction), whereas the polarization of photofragments recoiling at an angle θ will be reduced by $\cos\theta$, e) the electronic polarization of the atoms will be reduced by any nonzero nuclear spins due to hyperfine depolarization [12], and f) there is little or no control of the photofragment polarization at a fixed photodissociation wavelength with respect to the recoil direction. Recent experimental results indicate that sufficient favorable examples exist so that points a), b), and c) are not insurmountable, and experimental velocity resolution solves point d). The ideas presented in this paper show how disadvantages e) and f) can be overcome, so as to produce highly-polarized photofragments from molecular photodissociation, and with external control of the polarization direction with respect to the recoil direction.

As an example, let us consider the three lowest excited states of Cl_2 and Br_2, the $A\,^3\Pi_u(1u)$, $B\,^3\Pi_u(0_u^+)$, and $C\,^1\Pi_u(1u)$ states. The A and C states (both having $|\Omega| = 1$) correlate to two ground state $^2P_{3/2}$ atoms (X_1 and X_2) described in the $|m_{X_1}, m_{X_2}\rangle$ basis as:

$$|\pm 1\rangle_A \xrightarrow{R\to\infty} \frac{1}{\sqrt{2}}\left(\left|\pm\frac{3}{2},\mp\frac{1}{2}\right\rangle + \left|\mp\frac{1}{2},\pm\frac{3}{2}\right\rangle\right), \tag{4}$$

$$|\pm 1\rangle_C \xrightarrow{R\to\infty} \left|\pm\frac{1}{2},\pm\frac{1}{2}\right\rangle. \tag{5}$$

The B state correlates to a ground state $^2P_{3/2}$ atom and an excited state $^2P_{1/2}$ atom as:

$$|0\rangle_B \xrightarrow{R\to\infty} \frac{1}{\sqrt{2}}\left(\left|+\frac{1}{2},-\frac{1}{2}\right\rangle + \left|-\frac{1}{2},+\frac{1}{2}\right\rangle\right). \tag{6}$$

Adiabatic dissociation via either the A, B, or C states yields Cl or Br atoms with distinctly different polarizations. In fact, the detection of the photofragment polarization is a method for elucidating the reaction mechanism[13–15]. Selective excitation of one of the excited states can be achieved experimentally in many systems. For example, Br_2 was excited almost exclusively to the C state (using linearly polarized 355 nm light), and the photofragments were observed in the $m = \pm 1/2$ states only [16] (and were therefore cylindrically symmetric about the recoil direction), showing that the dissociation was adiabatic (Eq. 5). In contrast, when Cl_2 was also excited to the C state, the photofragments were

observed to also populate the $m = \pm 3/2$ states (about 20%) and the $m = \pm 1/2$ states (about 80%), showing nonadiabatic transfer from the C to the A state (about 40%) [16–19]. In addition, the angular momentum distribution was observed to break cylindrical symmetry about the recoil direction as a result of interference between the C and A state dissociation pathways. In general, coherent excitation of multiple dissociative states, or the formation of multiple pathways originating from a single dissociative state produce photofragments with a more complicated angular momentum distribution [13, 14]. However, here we will be mostly concerned with single-state adiabatic photodissociation.

The net result is that both Cl_2 and Br_2 photodissociation via the C state yields highly polarized atoms, but along different directions. The Br atoms are polarized along the recoil direction, whereas the Cl atoms are maximally aligned perpendicular to the recoil direction (perpendicular to the transition dipole moment). Similarly, large electronic polarizations have been produced or predicted for H, D, F, Cl, Br, I, O, and S atoms[20–29].

The photodissociation of Cl_2 has been used extensively for the production of hot, mono-energetic Cl atoms for studies of reactive scattering with hydrocarbons [30–38]. However, in these studies, the electronic alignment of the Cl atoms has been largely ignored. There are at least two reasons for this. First, despite the high degree of electronic alignment produced by the photodissociation, this alignment is reduced by nearly a factor of 4 due to nuclear hyperfine depolarization; after this reduction, the *maximal* error of ignoring the electronic alignment on the differential cross section measurements is about 15%, which necessarily has been considered negligible. Second, the chlorine atom alignment, in this case, is fixed with respect to the recoil direction, and so there was no spatial control of the atomic alignment in these experiments. We examine this depolarization mechanism in more detail, to see how it can be useful and not just detrimental.

There are several processes by which the non-nuclear angular momentum, J, of atoms or molecules can become promptly polarized (on a timescale much faster than the hyperfine interaction with the nuclear spin). For example, J can become polarized by pulsed-laser excitation, by a photodissociation, or chemical reaction. The polarization of J can be described by the polarization parameters $A_q^{(k)}(J,t)$. The time-dependent depolarization of J by nuclear spin I (when the hyperfine structure is not experimentally resolved) has been shown to be expressed by a k-dependent depolarization factor [39–42]:

$$A_q^{(k)}(J,t) = G^{(k)}(J,t)\, A_q^{(k)}(J,t=0), \tag{7}$$

where

$$G^{(k)}(J,t) = \sum_{F,F'} \frac{(2F'+1)(2F+1)}{2I+1} \begin{Bmatrix} F' & F & k \\ J & J & I \end{Bmatrix}^2 \cos[(E_{F'} - E_F)t/\hbar] \tag{8}$$

and where I and J are coupled to give total angular momentum F, with total energy E_F. For $t = 0$, $G^{(k)}(J,t) = 1$, and subsequently decreases at later times. This loss of polarization of J causes a gain in polarization of I (which is initially unpolarized). In a similar fashion, the time-dependent polarization of I can be expressed by a k-dependent polarization factor [42] multiplied by the *original* polarization of J:

$$A_q^{(k)}(I,t) = H^{(k)}(I,t)\, A_q^{(k)}(J, t=0), \tag{9}$$

where

$$H^{(k)}(I,t) = \frac{U_k(I)}{U_k(J)} \sum_{F,F'} \frac{(2F'+1)(2F+1)}{\sqrt{(2I+1)(2J+1)}} (-1)^{F-F'} \times \begin{Bmatrix} F' & F & k \\ J & J & I \end{Bmatrix} \begin{Bmatrix} F' & F & k \\ I & I & J \end{Bmatrix} \cos[(E_{F'} - E_F)t/\hbar]. \tag{10}$$

For $t = 0$, $H^{(k)}(I,t) = 0$, and subsequently increases at later times. Conservation of the projection of angular momentum $\langle m \rangle$ between J and I yields (for $k = 1$) [42]:

$$G^{(1)}(J,t) + \sqrt{\frac{I(I+1)}{J(J+1)}}\, H^{(1)}(I,t) = 1. \tag{11}$$

More general polarization factors for two nuclei I_1 and I_2 have been presented for the case of hierarchical coupling [42], and equations for non-hierarchical coupling will be presented elsewhere [43].

We present specific examples of how ^{35}Cl atom nuclei can be aligned or oriented following the optical excitation HCl and subsequent photodissociation after an appropriate time delay. For example, pulsed infrared excitation of H^{35}Cl($v = 0, J = 0$) with linearly polarized light yields H^{35}Cl($v = 1, J = 1, m = 0$) at time $t = 0$. This polarization is transferred to the ^{35}Cl nuclear spin. The time-dependence of the populations of the nuclear m states can be expressed in terms of the $A_0^{(k)}(I,t)$ [42, 44]:

$$p(J=3/2, m=+3/2) = \frac{1}{4}\Big(1 + 3\sqrt{\frac{3}{5}}A_0^{(1)} + \frac{5}{4}A_0^{(2)} + \frac{\sqrt{15}}{2}A_0^{(3)}\Big), \tag{12a}$$

$$p(J=3/2, m=+1/2) = \frac{1}{4}\Big(1 + \sqrt{\frac{3}{5}}A_0^{(1)} - \frac{5}{4}A_0^{(2)} - \frac{3\sqrt{15}}{2}A_0^{(3)}\Big), \tag{12b}$$

$$p(J=3/2, m=-1/2) = \frac{1}{4}\Big(1 - \sqrt{\frac{3}{5}}A_0^{(1)} - \frac{5}{4}A_0^{(2)} + \frac{3\sqrt{15}}{2}A_0^{(3)}\Big), \tag{12c}$$

$$p(J=3/2, m=-3/2) = \frac{1}{4}\Big(1 - 3\sqrt{\frac{3}{5}}A_0^{(1)} + \frac{5}{4}A_0^{(2)} - \frac{\sqrt{15}}{2}A_0^{(3)}\Big). \tag{12d}$$

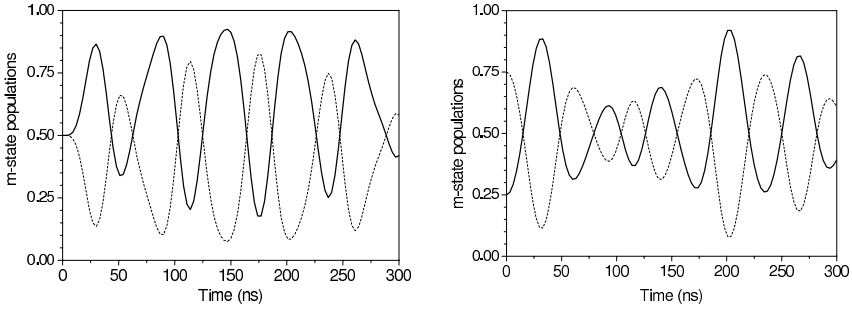

FIG. 1: The time-dependence of the m-state populations of the ^{35}Cl nuclear spins in the H^{35}Cl(v, J) molecules following pulsed optical excitation at $t = 0$ from H^{35}Cl$(v = 0, J = 0)$ for a) the $|m| = 1/2$ (solid line) and $|m| = 3/2$ (dashed line) states of H^{35}Cl$(v, J = 1, m = 0)$, and b) the $m = 3/2$ (solid line) and the sum of the $|m| = 1/2$ and $m = -3/2$ states (dashed line) states of H^{35}Cl$(v, J = 2, m = 2)$.

In Fig. 1a we show (using Eqs. 9, 10 and 12, and the hyperfine structure given by Kaiser [45]) how the m-state populations of $|m| = 3/2$ and $|m| = 1/2$ of the ^{35}Cl nuclear spin vary with time (note that for the timescales shown, effects of the H atom nuclear spin can be neglected, so only a single nuclear spin $I = 3/2$ is taken into account). At $t = 0$, these populations are each 0.5 (which is the case for unpolarized spins). At about 150 ns, the $|m| = 1/2$ population increases to more than 90%, whereas the complementary $|m| = 3/2$ population decreases to less than 10%. Prompt photodissociation at this point will yield highly aligned ^{35}Cl nuclei; typical photodissociation cross sections are of the order $\sigma_{\rm abs} \approx 10^{-18}$ cm^2, so that these transitions can be saturated with commercial pulsed lasers. A second, similar, example is the preparation of H^{35}Cl$(v, J = 2, m = 2)$ using Raman pumping. In Fig. 1b we show the time dependence of the population of the $m = +3/2$ ^{35}Cl spin state, and also the sum of the remaining three nuclear spin states ($|m| = 1/2$ and $m = -3/2$). At $t = 0$, the ^{35}Cl spin is unpolarized, so each of the four m states has a population of 1/4. We see that at about $t = 32$ or 205 ns the population of the $m = +3/2$ state has increased to about 90%. Prompt photodissociation at this point will yield highly oriented ^{35}Cl nuclei. These polarized atoms can be used on short timescales, for which the collisional depolarization effects are not significant.

The example of HCl illustrates the power of these techniques, however the photodissociation of hydrogen halides are not a good source of fast halide atoms (necessary for some applications, such as photo-initiated reactions in a bulb). The halogen or interhalogen molecules are much more promising as potential sources of polarized hot-atom sources; however, for this direction of be explored, appropriate optical excitation schemes must be found (such as vibrational or

electronic excitation), and the photofragment polarization from the photodissociation of these excited states must be quantified.

We have shown how photodissociation can yield highly electronically polarized atoms, and how optical excitation (followed by photodissociation) can yield atoms with highly polarized nuclear spins. In combination, these two techniques can be used to produce highly polarized atoms which will be in nearly pure states so that they will no longer depolarize significantly, and whose polarization can be controlled by the polarization of the excitation lasers. Furthermore, the density achievable is close to the density of the parent molecule, and can exceed 10^{16} atoms/cm^3, which are orders of magnitude larger than existing techniques.

Acknowledgements. We gratefully acknowledge support from the grant P.O. Education-Pythagoras of the Hellenic Ministry of Education, and the E.U. grants HPRI-CT-1999-00074 (Improving Human Potential-Transnational Access to major Research Infrastructures) and HPRN-CT-2002-00183 (PICNIC).

---

[1] E. Steffens and W. Haeberli, Rep. Prog. Phys. **66**, 1887 (2003).
[2] S. G. Redsun, R. J. Knize, G. D. Cates and W. Happer, Phys. Rev. A **42**, 1293 (1990).
[3] C. T. Rettner and R. N. Zare, J. Chem. Phys. **77**, 2416 (1982)
[4] M. S. Albert, G. D. Cates, B. Driehuys, W. Happer, B. Saam, C. S. Springer and A. Wishnia, Nature **370**, 199 (1994).
[5] W. Gerlach and O. Stern, Ann. der Phys. **74**, 673 (1924).
[6] K. Zapfe, K. Braun, H.-G. Gaul, M. Griesner, B. Povh, M. Rall, E. Steffens, F. Stock, J. Tonhouser, C. Montag, F. Rathmann, D. Fick and W. Haeberli, Rev. Sci. Instrum. **66**, 28 (1995).
[7] W. Happer, Rev. Mod. Phys. **44**, 169 (1972).
[8] K. S. E. Eikema, J. Walz and T. W. Hnsch, Phys. Rev. Lett. **83**, 3828 (1999)
[9] E. Babcock, I. Nelson, S. Kadlecek, B. Driehuys, L. W. Anderson, F. W. Hersman and T.G.Walker, Phys. Rev. Lett. **91**, 123003 (2003).
[10] S. Appelt, A. Ben-Amar Baranga, C. J. Erickson, M. V. Romalis, A. R. Young and W. Happer, Phys. Rev. A. **58**, 1412 (1998).
[11] R. J. van Brunt and R. N. Zare, J. Chem. Phys. **48**, 4304 (1968).
[12] A. J. Orr-Ewing, W. R. Simpson, T. P. Rakitzis and R.N. Zare, Isr. J. Chem. **34**, 95 (1994).
[13] L. D. A. Siebbeles, M. Glass-Maujean, O. S. Vasyutinskii, J. A. Beswick and O. Roncero, J. Chem. Phys. **100**, 3610 (1994).
[14] T. P. Rakitzis and R. N. Zare, J. Chem. Phys. **110**, 3341 (1999).
[15] G. G. Balint-Kurti, A. J. Orr-Ewing, J. A. Beswick, A. Brown and O.S. Vasyutinskii, J. Chem. Phys. **116**, 10760 (2002).
[16] T. P. Rakitzis and T. N. Kitsopoulos, J. Chem. Phys. **116**, 9228 (2002).
[17] A. S. Bracker, E. R. Wouters, A. G. Suits and O. S. Vasyutinskii, J. Chem. Phys. **110**, 6749 (1999).
[18] T. P. Rakitzis, S. A. Kandel, A. J. Alexander, Z. H. Kim and R. N. Zare, J. Chem.

Phys. **110**, 3351 (1999).
[19] A. J. Alexander, Z. H. Kim, S. A. Kandel, R. N. Zare, T. P. Rakitzis, Y. Asano and S. Yabushita, J. Chem. Phys. **113**, 9022 (2000).
[20] T. P. Rakitzis, S. A. Kandel, A. J. Alexander, Z. H. Kim and R.N. Zare, J. Chem. Phys. **110**, 3351 (1999).
[21] T. P. Rakitzis, P. C. Samartzis, R. L. Toomes and T. N. Kitsopoulos, J. Chem. Phys. **121**, 7222 (2004).
[22] Y. Mo, H. Katayanagi, M. C. Heaven and T. Suzuki, Phys. Rev. Lett. **77**, 830 (1996).
[23] A. T. J. B. Eppink, D. H. Parker, M. H. M. Janssen, B. Buijsse and W. J. van der Zande, J. Chem. Phys. **108**, 1305 (1998).
[24] T. P. Rakitzis *et al.*, Chem. Phys. Lett. **354**, 115 (2002).
[25] K. O. Korovin, B. V. Picheyev, O. S. Vasyutinskii, H. Valipour and D. Zimmermann, J. Chem. Phys. **112**, 2059 (2000).
[26] J. M. Teule, G. A. Groenenboom, D. W. Neyer, D. W. Chandler and M. H. M. Janssen, Chem. Phys. Lett. **320**, 177 (2000).
[27] T. Suzuki, H. Katayanagi, Y. Mo and K. Tonokura, Chem. Phys. Lett. **256**, 90 (1996).
[28] A. Brown, G. G. Balint-Kurti, O. S. Vasyutinskii, J. Phys. Chem. A **108**, 7806 (2004).
[29] A. Brown, J. Chem. Phys. **122**, 084301 (2005).
[30] W. R. Simpson, T. P. Rakitzis, S. A. Kandel, A. J. Orr-Ewing and R. N. Zare, J. Chem. Phys. **103**, 7313 (1995).
[31] S. A. Kandel, T. P. Rakitzis, T. Lev-On and R. N. Zare, J. Chem. Phys. **105**, 7550 (1996).
[32] A. J. Orr-Ewing, W. R. Simpson, T. P. Rakitzis, S. Kandel and R. N. Zare, J. Chem. Phys. **106**, 5961 (1997).
[33] M. J. Bass, M. Brouard, C. Vallance, T. N. Kitsopolulos, P. C. Samartzis and R. Toomes, J. Chem. Phys. **119**, 7168 (2003).
[34] M. J. Bass, M. Brouard, A. P. Clark, C. Vallance and B. Martnez-Haya, Phys. Chem. Chem. Phys. **5**, 856 (2003).
[35] M. J. Bass, M. Brouard, C. Vallance, T. N. Kitsopolulos, P. C. Samartzis and R. Toomes, J. Chem. Phys. **121**, 7175 (2004).
[36] S. Rudic, C. Murray, J. N. Harvey and A. J. Orr-Ewing, J. Chem. Phys. **120**, 186 (2004).
[37] S. Rudic, C. Murray, J. N. Harvey and A.J. Orr-Ewing, Phys. Chem. Chem. Phys. **5**, 1205 (2003).
[38] K. A. Cowen, Y. Yu-Fong, K. T. Lorentz, B. D. Koplitz, in Proc. SPIE 2548, 350, Laser Techniques for State-Selected and State-to-State Chemistry III, ed. by John W. Hepburn (1995).
[39] K. Blum, Density Matrix Theory and Applications (Plenum Press, New York, 1981).
[40] R. N. Zare, Angular Momentum (Wiley, New York, 1988).
[41] R. Altkorn, R. N. Zare and C.H. Greene, Mol. Phys. **55**, 1 (1985).
[42] T. P. Rakitzis, Phys. Rev. Lett. **94**, 083005 (2005).
[43] L. Rubio-Lago, D. Sofikitis and T. P. Rakitzis, in preparation.
[44] A. J. Orr-Ewing, R. N. Zare, Annu. Rev. Phys. Chem. **45**, 315 (1994).
[45] E. W. Kaiser, J. Chem. Phys. **53**, 1686 (1970).

G. G. Balint-Kurti and M. P. de Miranda (eds.)
Vector Correlation and Alignment in Chemistry

Velocity map imaging studies of O_2 and OH molecular photodissociation

David H. Parker
Department of Molecular and Laser Physics, University of Nijmegen, Toernooiveld 1, 6525 ED Nijmegen, The Netherlands

Over the past few years a new generation of photodissociation experiments has begun where full quantum state distributions including the M_J quantum number of product atoms are determined. The spatial polarization of the atomic photofragment is measured in the laboratory frame and transformed into the molecule based M_J distribution, which yields a very detailed insight in the photoabsorption step and subsequent non-adiabatic processes leading to the final products. In many previous photodissociation experiments this polarization information was either ignored or it could not be reliably extracted from the data. Following new experimental developments such as the combination of ion imaging [1] with velocity mapping [2] and enhanced by experimental slicing techniques [3] such as delayed-field slicing [4], it is now possible to reliably extract a wide range of polarization parameters [5]. These parameters are often interpreted in a formalism following the fully quantum treatment of Siebbeles and coworkers [6]. The information gained, such as whether or not two or more electronic states are optically excited and whether they act coherently or incoherently, is so insightful that in many cases it will be necessary in the future to repeat previous photodissociation studies of many molecules.

Recently, we have used the delayed field slicing methlod [4] to probe the $O(^3P_J) + O(^1D)$ photo-fragment angular distribution and polarization following the photodissociation of the O_2 and OH molecules. We have previously reported [7] one of the most extreme product alignment effects observed thus far, for the photodissociation of O_2 in the continuum of the $B^3\Sigma_u^-$ state, the upper state of the Schumann-Runge band. $O(^1D)$ atoms were observed with maximal population in the $J = 2, M_J = 0$ state when exciting a single rotational state of O_2 in the $b^1\Sigma_g^+$ state via the forbidden b-B transition. This extreme alignment is again observed in recent experiments when exciting O_2 directly from the $X^3\Sigma_g^-$ ground electronic state using 157 nm radiation, and when starting from vibrationally excited levels of the ground electronic state followed by photoexcitation to the same Schumann-Runge continuum. Houston and coworkers [8] also observed strong $O(^1D)$ alignment in an O_2 photodissociation study at the high energy end of the Schumann-Runge continuum. A full polarization anal-

ysis including alignment and orientation effects at 157 nm will be described in a future article [9]. This photodissociation process is quite striking in that the same extreme polarization is found at all dissociation energies up to at least $15{,}000\,\mathrm{cm}^{-1}$ above threshold for the *second* ($O^3P + O^1D$) dissociation limit.

Studies of the *first* ($O^3P + O^3P$) dissociation limit reached via the Herzberg continuum, reveal totally different dynamics, ranging from adiabatic near threshold to diabatic only slightly above threshold [10]. A previous study by our group [11] has shown that deconvolution of the Herzberg continuum is possible using the $O(^3P_J)$ quantum yields and angular distributions. Product polarization information was not available because a single laser was used to both photodissociate O_2 and photoionize the $O(^3P_J)$ atom using (2+1) REMPI. Van Vroonhoven and Groenenboom [12] have reported a semi-classical study which provides a deeper interpretation of this data. It was clear from their analysis, however, that a fully quantum analysis is necessary. In a more recent experimental study using a velocity sensitive time-of-flight method by Alexander *et al.* [13] showed that the $O(^3P)$ atoms are both aligned and oriented, indicating interference effects in a coherent absorption process. We have now carried out new experiments [10] showing that pulsed-field slicing is especially powerful in near-threshold photodissociation of O_2. We find that on photodissociation above $\sim 240\,\mathrm{nm}$ it is possible when using $O(^3P_2)$ detection to resolve the $O(^3P_2)$ and $O(^3P_1)$ products channels. These show strongly differing angular distributions. A full interpretation of the data will require a fully quantum dynamics analysis.

A similar, wide-ranging study of molecular photodissociation has been carried out for OH and OD [14], (and for the related SH, SD molecules [15]). The radicals are produced in an electrical discharge and state selected and focused using an electrostatic hexapole. Direct photodissociation is possible for OH only with VUV excitation, but the excited state repulsive curve can reached using UV light by starting from vibrationally excited ground-state molecules produced in the pulsed discharge. One-laser studies at several different dissociation/detection wavelengths are shown to yield a wide range of photo-dynamical information on the potential energy curves involved. This data is compared and agrees well with predictions using the sudden limit model and recent ab-initio potential energy curves from the Theoretical Chemistry group of Groenenboom in Nijmegen for OH/OD [16] and for SH/SD [17]. Predissociation of OH excited to different rovibrational levels of the A-state in a two-laser configuration with full polarization studies of the product $O(^3P)$ atoms have also been measured [14] and compared with results from a recent high-resolution Rydberg tagging experiments on the OH [18] and SH [19] systems. For both OH/OD and SH/SD our experiments, and the Rydberg tagging experiments, find no evidence of absorption and interference from the $A^2\Sigma^+$ electronic state above threshold for the $O(S)(^1D)$ dissociation limit, as predicted by Lee [20] for OH, and by Freed and coworkers for the SH radical [21]. Recent ab-initio calculations by Groenenboom and coworkers[16, 17] indicate that the A-state absorption cross section is negligible

at these excitation energies.

---

[1] D. W. Chandler and P. L. Houston, J. Chem. Phys. **87**, 1445 (1987).
[2] A. T. J. B. Eppink and D. H. Parker, Rev. Sci. Instr. **68**, 3477 (1997).
[3] C. R. Gebhardt, T. P. Rakitzis, P. C. Samartzis, V. Ladopoulos, T. N. Kitsopoulos, Rev. Sci. Instrum. **72**, 3848 (2001).
[4] D. A. Chestakov, M. Wu, G. Wu, A. T. J. B. Eppink, D. H. Parker and T. N. Kitsopolous, J. Phys. Chem. A **108**, 8100 (2004).
[5] *Imaging in Chemical Dynamics* (eds. A. G. Suits and R. E. Continetti), ACS Symp. Ser. 770, American Chemical Society, Washington, DC, 2001.
[6] L. D. A. Siebbeles, M. Glass-Maujean, O. S. Vasyutinskii, J. A. Beswick and O. Roncero, J. Chem. Phys. **100**, 3610 (1994).
[7] A. T. J. B. Eppink, B. Buijsse, M. H. M. Janssen, W. J. van der Zande and D. H. Parker, J. Chem. Phys. **108**, 1305 (1998).
[8] H. M. Lambert, A. A. Dixit, E. W. Davis and P. L. Houston, J. Chem. Phys. **121**, 10437 (2004).
[9] S. Wu, W. van der Zande, D. H. Parker, X. Yang, G. Groenenboom, C. Vallance and O. Vasytinskii, work in progress.
[10] D. Chestakov, D. H. Parker and G. Groenenboom, work in progress.
[11] B. Buijsse, W. J. van der Zande, A. T. J. B. Eppink, D. H. Parker, B. R. Lewis and S. T. Gibson, J. Chem. Phys. **108**, 7229 (1998).
[12] M. C. G. N. van Vroonhoven and G. C. Groenenboom, J. Chem. Phys. **116**, 1954 (2002); *ibid*, **116**, 1965 (2002).
[13] A. J. Alexander, Z. H. Kim and R. N. Zare, J. Chem. Phys. **118**, 10566 (2003).
[14] D. Radenovic and D. H. Parker, work in progress.
[15] I. Anton, L. Janssen, S. M. Wu, D. Radenovic and D. H. Parker, work in progress.
[16] M. van der Loo and G. Groenenboom, J. Chem. Phys. (2005), in press.
[17] L. Janssen, M. van der Loo and G. Groenenboom, work in progress.
[18] W. Zhou, Y. Yuan and J. Zhang, J. Chem. Phys. **119**, 9989 (2004).
[19] W. Zhou, Y. Yuan, S. Chen and J. Zhang, J. Chem. Phys. (2005), in press.
[20] S. Lee, J. Chem. Phys. **111**, 6407 (1999).
[21] S. Lee, H. Sun, B. Kim and K. F. Freed, J. Chem. Phys. **114**, 5537(2001); *ibid*, **116**, 10656 (2002).

G. G. Balint-Kurti and M. P. de Miranda (eds.)
Vector Correlation and Alignment in Chemistry

Polarization of photofragments fluorescence: the semiclassical treatment

J. Alberto Beswick
IRSAMC, Université Paul Sabatier, Toulouse, France

I. INTRODUCTION

Since the pioneering theoretical prediction by van brunt and Zare in 1968 [1], the photofragments fluorescence-polarization has been the subject of numerous theoretical and experimental work. The polarization of Lyman-α fluorescence following photodissociation of molecular hydrogen for instance, has been studied in detail since the system allows precise theoretical *ab initio* calculations. In particular, for energies above the H(2ℓ) + H($1s$) dissociation limit, the theory [2, 3] predicted oscillations of the polarization ratio as a function of the excess energy which have been observed experimentally [4]. Recently [5], the polarization anisotropy of Lyman-α fluorescence in the photodissociation of the doubly excited states of H_2 has been measured in the 27-38 eV range. This states bring up a case which has not been considered before namely, the production of H($2p\sigma$)+H($2p\pi$) fragments, i.e. the two fragments are excited with and have angular momentum different from zero.

We show that this process, as well as many others can be calculated by using the simple semiclassical treatment in terms of absorption and emitting oscillators.

II. SEMICLASSICAL MODEL

In the semiclassical model, absorption $\boldsymbol{\mu}_a$ and emission $\boldsymbol{\mu}_e$ classical dipoles pointing in the direction of the quantum transition dipole moments, are considered. For a given electronic transition and a fixed orientation of the molecule the probability for excitation is proportional to $|\boldsymbol{\mu}_a.\boldsymbol{\epsilon}_i|^2$, while for the emission it is proportional to $|\boldsymbol{\mu}_e.\boldsymbol{\epsilon}_f|^2$. The fluorescence intensity with polarization $\boldsymbol{\epsilon}_f$ will then be given by $I(\boldsymbol{\epsilon}_f) \propto \langle|(\boldsymbol{\mu}_a.\boldsymbol{\epsilon}_i)(\boldsymbol{\mu}_e.\boldsymbol{\epsilon}_f)|^2\rangle$ where $\langle\cdots\rangle$ denotes the average over the initial orientation of the molecule with respect to the laboratory $OXYZ$ axis.

The following experimental geometry is chosen. The incident light propagates

along the OX axis with linear polarization along OZ and the detector is along the OY axis. Thus, we have $\boldsymbol{\epsilon}_i = \boldsymbol{Z}$, $(\boldsymbol{\epsilon}_f)_\parallel = \boldsymbol{Z}$ and $(\boldsymbol{\epsilon}_f)_\perp = \boldsymbol{X}$. The intensities parallel and perpendicular will then be given by $I_\parallel \propto \left\langle |(\boldsymbol{\mu}_a.\boldsymbol{Z})(\boldsymbol{\mu}_e.\boldsymbol{Z})|^2 \right\rangle$, $I_\perp \propto \left\langle |(\boldsymbol{\mu}_a.\boldsymbol{Z})(\boldsymbol{\mu}_e.\boldsymbol{X})|^2 \right\rangle$, respectively. Since $\boldsymbol{\mu}_a$ and $\boldsymbol{\mu}_e$ are fixed with respect to the molecule $Oxyz$ frame, the intensity will be proportional to the average of $(\Phi_{Zg}\Phi_{Zg'})^2$ and $(\Phi_{Zg}\Phi_{Xh})^2$, with $(q, h = x, y, z)$, where Φ_{Fg} are the direction cosine relating the laboratory to the molecule frames. For linear molecules,

$$\begin{pmatrix} X \\ Y \\ Z \end{pmatrix} = \boldsymbol{\Phi}_{Fg} \begin{pmatrix} x \\ y \\ z \end{pmatrix} = \begin{pmatrix} \cos\theta\,\cos\phi & -\sin\phi & \sin\theta\,\cos\phi \\ \cos\theta\,\sin\phi & \cos\phi & \sin\theta\,\sin\phi \\ -\sin\theta & 0 & \cos\theta \end{pmatrix} \begin{pmatrix} x \\ y \\ z \end{pmatrix} \tag{1}$$

It is possible to include interference effects due to coherent excitation of different continua in the semiclassical model. For two continua, for instance, we write

$$\begin{aligned} I(\boldsymbol{\epsilon}_f) &\propto \left\langle \left| (\boldsymbol{\mu}_a.\boldsymbol{\epsilon}_i)(\boldsymbol{\mu}_e.\boldsymbol{\epsilon}_f) + (\boldsymbol{\mu}'_a.\boldsymbol{\epsilon}_i)(\boldsymbol{\mu}'_e.\boldsymbol{\epsilon}_f) \right|^2 \right\rangle \\ &= \left\langle |(\boldsymbol{\mu}_a.\boldsymbol{\epsilon}_i)(\boldsymbol{\mu}_e.\boldsymbol{\epsilon}_f)|^2 \right\rangle \\ &+ \left\langle |(\boldsymbol{\mu}'_a.\boldsymbol{\epsilon}_i)(\boldsymbol{\mu}'_e.\boldsymbol{\epsilon}_f)|^2 \right\rangle + 2\,\mathrm{Re}\left[\left\langle (\boldsymbol{\mu}_a.\boldsymbol{\epsilon}_i)^*(\boldsymbol{\mu}_e.\boldsymbol{\epsilon}_f)^*(\boldsymbol{\mu}'_a.\boldsymbol{\epsilon}_i)(\boldsymbol{\mu}'_e.\boldsymbol{\epsilon}_f) \right\rangle \right] \end{aligned} \tag{2}$$

It should be noted however that interference can only occur for processes concerning the same initial state and final dissociative continua giving the same final state of fragment B. Thus, for instance, it is possible to have interference between the two processes

$$\begin{aligned} &\mathrm{AB}(\Sigma) \xrightarrow{h\nu} \mathrm{AB}^*(\Sigma) \rightarrow \mathrm{A}^*(p\sigma) + B(\sigma);\ \mathrm{A}^*(p\sigma) \xrightarrow{h\nu'} \mathrm{A}(s) \\ &\mathrm{AB}(\Sigma) \xrightarrow{h\nu} \mathrm{AB}^*(\Pi) \rightarrow \mathrm{A}^*(p\pi) + B(\sigma);\ \mathrm{A}^*(p\pi) \xrightarrow{h\nu'} \mathrm{A}(s) \end{aligned} \tag{3}$$

with the result

$$\mathcal{P} = \frac{2\,|M_\parallel|^2 + 7\,|M_\perp|^2 + 3\left(M_\parallel\,M_\perp^* + M_\parallel^*\,M_\perp\right)}{4\,|M_\parallel|^2 + 9\,|M_\perp|^2 + \left(M_\parallel\,M_\perp^* + M_\parallel^*\,M_\perp\right)} \tag{4}$$

Another possible interference is between the two processes

$$\mathrm{AB}(\Sigma) \xrightarrow{h\nu} \mathrm{AB}^*(\Pi) \rightarrow \mathrm{A}^*(p\sigma) + B(\pi);\ \mathrm{A}^*(p\sigma) \xrightarrow{h\nu'} \mathrm{A}(s) \tag{5}$$

$$\mathrm{AB}(\Sigma) \xrightarrow{h\nu} \mathrm{AB}^*(\Sigma) \rightarrow \mathrm{A}^*(p\pi) + B(\pi);\ \mathrm{A}^*(p\pi) \xrightarrow{h\nu'} \mathrm{A}(s) \tag{6}$$

with the result

$$\mathcal{P} = -\frac{2\left(|M_\parallel|^2 + |M_\perp|^2\right) - 3\left(M_\parallel\, M_\perp^* + M_\parallel^*\, M_\perp\right)}{6\left(|M_\parallel|^2 + |M_\perp|^2\right) + \left(M_\parallel\, M_\perp^* + M_\parallel^*\, M_\perp\right)} \tag{7}$$

The corresponding quantum results have been obtained by the standard multipole treatment of alignment and orientation of photofragments [6, 7]. The agreement between quantum and semiclassical results is perfect for all individual photodissociation processes, i.e. without interference. For the interference terms Eq. (4) is exactly equal to the quantum result. On the other hand, in the interference terms of Eq. (7) there is a sign difference with respect to the quantum result. Everything looks like if in Eq. (2) the + sign have to be replaced by −. It should be noted that the process $\mathrm{AB}(\Sigma^+) \rightarrow \mathrm{AB}^*(\Sigma^*) \rightarrow \mathrm{A}^*(p\pi) + B(\pi)$; $\mathrm{A}^*(p\pi) \rightarrow \mathrm{A}(s)$ correspond to a entangled state of the fragments: when A has component Ω_A = +1 B has Ω = -1, and viceversa. Thus the wavefunction does not factorize as a product of a wavefunction of A and a wavefunction of B (entangled state). Whether this could be the reason for the sign problem in the semiclassical treatment or a calculation mistake, it remains an open question.

---

[1] R. V. Brunt and R. Zare, J. Chem. Phys. **48**, 4304 (1968).
[2] M. Glass-Maujean and J.A. Beswick, Phys. Rev. A **36**, 1170 (1987).
[3] M. Glass-Maujean and J.A. Beswick, J. Chem. Soc. Faraday Trans. 2 **85**, 983 (1989).
[4] E. Flemming, W. Wilhelmi, H. Schmoranzer, and M. Glass-Maujean, J. Chem. Phys. **103**, 4090 (1995).
[5] M. Glass-Maujean, R. Kneip, E. Flemming, and H. Schmoranzer, Eur. J. Phys. (2005), in press.
[6] L. Siebbeles, M. Glass-Maujean, O. Vasyutinskii, J.A. Beswick, and O. Roncero, J.Chem.Phys. **100**, 3610 (1994).
[7] J. Beswick, to be published.

G. G. Balint-Kurti and M. P. de Miranda (eds.)
Vector Correlation and Alignment in Chemistry

Product angular and alignment distributions in photodissociation from Rydberg states: NO, O_2 and N_2O

Paul L. Houston
Baker Laboratory of Chemistry, Cornell University, Ithaca, NY 14853 USA

I. TWO-PHOTON EXCITATION AND DISSOCIATION THROUGH NO RYDBERG LEVELS

Despite reports of excitation spectra and product analysis, it is only recently that product imaging has been used to investigate angular distributions of the products of NO predissociation from Rydberg states. We have investigated dissociation of NO Rydberg states using two-photon excitation to populate the $8d\pi^-(v=1)$, the $6d\pi^-(v=1)/5s\sigma(v=3)$, and the $5s\sigma(v=2)$ Rydberg levels in jet-cooled NO at wavelengths near 265, 270 and 278 nm, respectively. These states, excited at relatively low powers, show rotational resolution. Velocity mapped images of the dissociation product $O(^3P_2)$ were recorded at various rotational lines in these regions, and the resulting angular distributions were compared to quantum mechanical theoretical calculations. Not only do the angular distributions aid in confirming spectral assignments, they also distinguish between Σ, Π, and Δ intermediate states in the two-photon excitation.

Our spectra of jet-cooled NO can be recorded either by monitoring the NO^+ created by a third photon following two-photon excitation of the Rydberg or by monitoring the O atom produced by the dissociation and detected by a second laser tuned to the 2+1 ionization wavelength near 226 nm. In the case of the $8d\pi^-(v=1)$ level and the $5s\sigma(v=2)$ level, our spectra are very similar to those obtained earlier by Pratt *et al.* [1] The most interesting spectrum is one we assign to an overlap between the $6d\pi^-(v=1)$ and $5s\sigma(v=3)$ Rydbergs, as shown in Fig. 1. We were able to show that both transitions contribute and to confirm our spectral assignments by measuring the angular distribution of the products and comparing to the theoretical prediction.

The angular distribution expected following excitation of a selected rotational transition from case a coupling to case b coupling through an intermediate of case b is given by,

$$I(\theta) = \sum_M \left| D^{(2)}_{\Lambda',\varepsilon'\leftarrow\Lambda'',\varepsilon''}(J',N',J'',N'',M) \sum_{M_S} \begin{Bmatrix} \langle N'\Lambda', SM_S|J'M\rangle\, d^{J'}_{M\Lambda'}(\theta) \\ \pm\langle N'-\Lambda', SM_S|J'M\rangle\, d^{J'}_{M-\Lambda'}(\theta) \end{Bmatrix} \right|^2$$

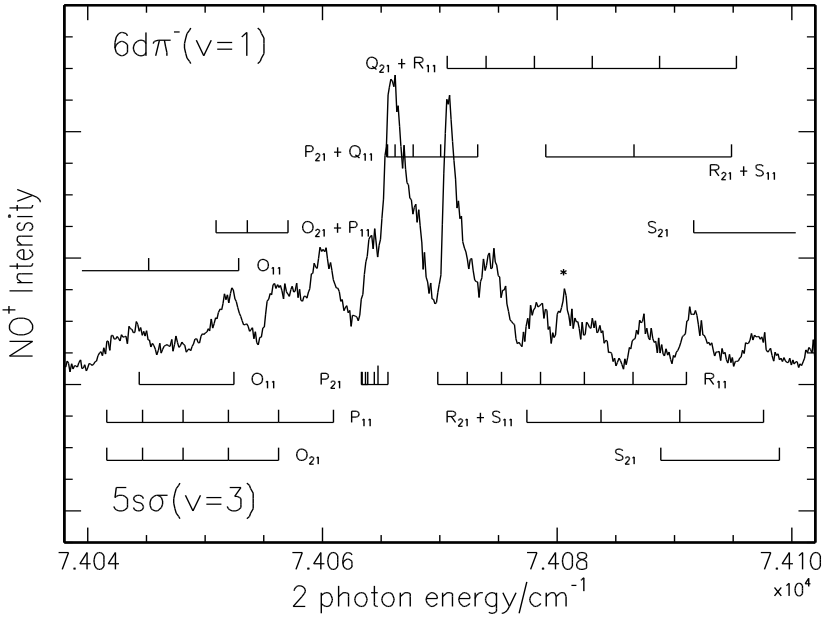

FIG. 1: Two-photon ionization spectra of NO as a function of the two-photon energy.Ionization of the $6d\pi^-(v=1)/5s\sigma(v=3)$ bands using 100% NO. Top assignments correspond to $6d\pi^-(v=1)$, while bottom assignments belong to $5s\sigma(v=3)$.

where M is the projection of the rotational angular momentum onto the direction of the linear polarization of the excitation laser, D is a line-strength factor, and the two terms in the second summation are Clebsch-Gordan factors multiplied by rotation matrices; the $+/-$ sign is used for positive/negative parity levels. The angular distribution is very sensitive to the rotational level and branch and to the symmetries of the intermediate electronic state in the two-photon excitation scheme, over which D is a summation.

Figure 2 shows the comparison between the calculated angular distributions based on the formula above and those measured following excitation to lines assigned to particular transitions. The good agreement between prediction and measurement gives confidence to our assignments. Not all assignments agreed so well, but all those that did not shared a particular intermediate and final level, thought to be perturbed. The angular distributions for this and for the other Rydberg levels studied could be fit only if it was assumed in the calculation that nearly all of the two-photon amplitude for the excitation went through an intermediate state of Π symmetry, probably the $C^2\Pi$ state.

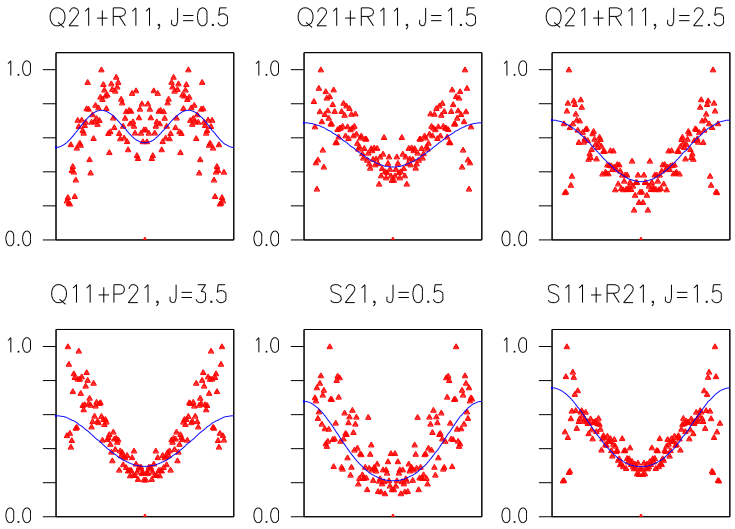

FIG. 2: Comparison between measured and predicted angular distributions. The x axis in all cases is from 0 to π radians.

II. QUANTUM YIELDS FOR PRODUCT FORMATION IN THE 120–133 nm PHOTODISSOCIATION OF O_2

Oxygen is a molecule of fundamental importance to atmospheric chemistry, but surprisingly little is known about its highly excited electronic states. We have studied the photodissociation of O_2 in the region from 120–133 nm by using product imaging. The spectrum in this region is dominated by transitions from the ground state u to the first three vibrational levels of the $E^3\Sigma_u^-$ state. As shown in Fig. 3, the $O(^1D) + O(^3P)$ channel is the only product channel observed by product imaging for dissociation at 124.4 nm; this is also true at 120.4 nm. The figure shows the velocity distributions of the $O(^1D)$ product (top) and the $O(^3P_2)$ product (bottom) for dissociation at 124.4 nm. Peaks in both panels 2 correspond to the production of the $O(^1D) + O(^3P)$ channel, but there are no peaks corresponding to other possible channels. Similar data was obtained concerning the velocity distribution of the $O(^1D)$ product for dissociation at 120.4 nm. Again, a peak in the distribution corresponds to production of $O(^1D)+O(^3P)$, but no peak is observed for the channel producing $O(^1D) + O(^1D)$. We conclude that the quantum yield for $O(^1D)$ production at both wavelengths is unity.

The $O(^1D_2)$ product is aligned in the molecular frame in such a way that its **J** vector is perpendicular to the relative velocity vector between the $O(^1D)$ and the

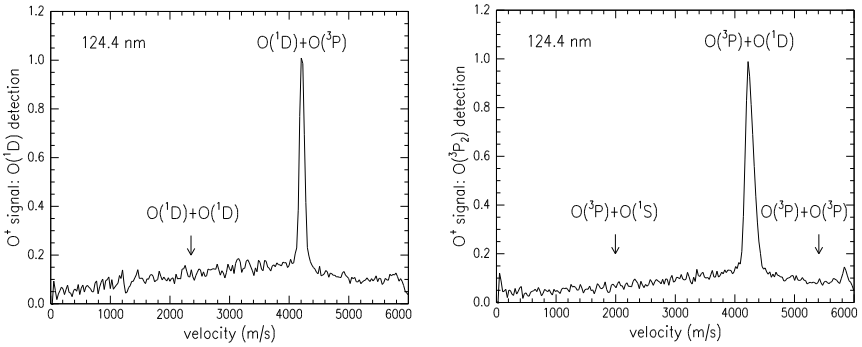

FIG. 3: Speed distributions of O(^1D) (left panel) and P(^3P) (right panel) produced in the 124.4 nm dissociation of O_2.

O(^3P). The repulsive part of the $O_2(E^3\Sigma_u^-)$ state is actually the continuation of the repulsive part of the $O_2(B^3\Sigma_u^-)$ state, which correlates to the observed $O(^1D) + O(^3P)$ products, as shown in Fig. 4. According to the Wigner-Witmer rules, the combination of ^1D and ^3P atoms to produce a Σ state can only occur with $m_J = 0$ or 1. This prediction is consistent with our finding that $m_J = 0$ is strongly preferred.

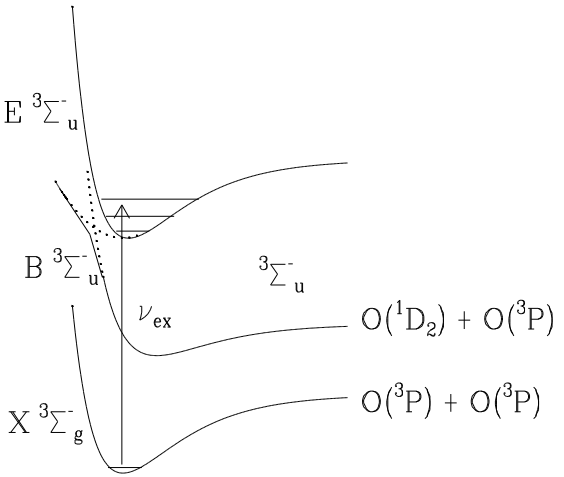

FIG. 4: Schematic diagram of O_2 X, B, and E states.

At a dissociation wavelength of 132.7 nm, both the $O(^1D) + O(^3P)$ and the $O(^3P) + O(^3P)$ channels are observed with branching ratios of 0.40 ± 0.08 and 0.60 ± 0.09, respectively. At 130.2 nm, the quantum yield for production of $O(^1D)$ is 0.76 ± 0.28.

III. PHOTODISSOCIATION OF N_2O NEAR 130 nm

Nitrous oxide is an important component of Earths natural atmosphere produced primarily by biological processes in soils and oceans. Mostly inert in the troposphere, it is transported to the stratosphere where it is destroyed both by photodissociation (at $\lambda \approx 200\,\text{nm}$), $N_2O + h\nu \rightarrow N_2(X\,^1\Sigma) + O(^1D)$ and by reaction with $O(^1D)$ produced either in the photodissociation or from the dissociation of ozone, $N_2O + O(^1D) \rightarrow N_2 + O_2$ and $\rightarrow NO + NO$. NO produced in the second reaction is the primary catalytic agent destroying stratospheric ozone in the natural atmosphere.

At shorter wavelengths, N_2O can be excited to the $C(^1\Pi)$ state near 145 nm or to the $D(^1\Sigma^+)$ state near 130 nm. The absorption coefficient for the latter transition is high, about 80 Mb ($1\,\text{Mb} = 10^{-18}\,\text{cm}^2$). Although dissociation process (1) near 200 nm has been extensively studied, that at shorter wavelengths is both more complex and less well understood. At 130 nm, the following channels are thought to be important:

$$N_2O + h\nu \rightarrow O(^1S) + N_2(X\,^1\Sigma) \quad (1)$$

$$\rightarrow N(^2D) + NO(X\,^2\Pi) \quad (2)$$

$$\rightarrow N(^2P) + NO(X\,^2\Pi) \quad (3)$$

$$\rightarrow O(^3P) + N_2(A\,^3\Sigma_u^+) \quad (4)$$

$$\rightarrow O(^3P) + N_2(B\,^3\Pi_g). \quad (5)$$

We have investigated channels (1)–(5) by using product imaging to detect the angular distributions for the five channels as well as the kinetic energy release for each of the product atoms or diatoms. The atomic products were probed by resonant $(1+1')$ ionization using ultraviolet excitation for the first step, while the diatomic products were probed by non-resonant ionization. Our work is part of a larger effort at Cornell to characterize this photodissociation process. Witinski, Ortiz-Suárez, and Davis have used oxygen Rydberg time-of-flight spectroscopy to study channels (4) and (5), with results that are in reasonable agreement with ours [2].

Figure 5 shows the total kinetic energy release for the $O + N_2$ products based on measurements of the $O(^1S)$, $O(^3P_0)$, $O(^3P_2)$, and N_2 products. In each case, conservation of momentum is assumed to determine the total kinetic energy release. The good match for the N_2 and $O(^3P)$ peaks in the lower panel shows

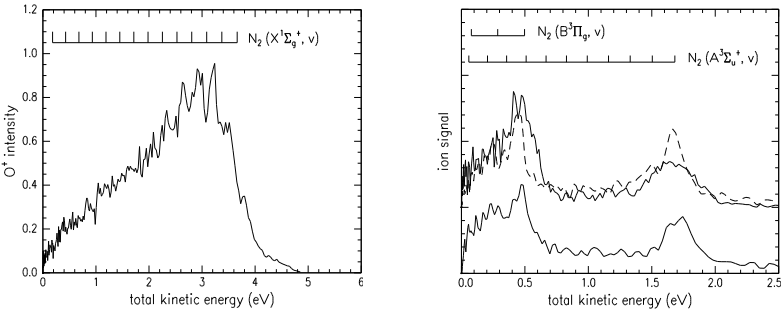

FIG. 5: Total kinetic energy released for $O+N_2$ products from the dissociation of N_2O at 130.2 nm. Left: $O(^1S)$. Right: $O(^3P_2)$ top solid curve; $O(^3P_0)$ top dashed curve; N_2^+ bottom curve.

that these are indeed momentum matched. Similar data was obtained for the N+ NO channel, where $N(^2D)$, $N(^2P)$, and NO were probed. In each of these cases, the energy release data provides information about the vibrational distribution of the diatomic fragment.

Information about the branching ratio between various channels has also been obtained. The ratio of O+ and NO+ can be converted to a branching ratio between the dissociation channels leading to $O(^3P)+N_2$ vs. N+NO by calibrating against the O^+ and NO^+ peaks obtained from the dissociation of NO_2 at 355 nm, assuming that the vibrational distributions for NO in the NO_2 dissociation and the N+NO products are not too different. The reaction appears to favor the $O(^3P)+N_3$ channel by a ratio of 1.4 ± 0.5. Vacuum ultraviolet line strengths for $O(^3P)$ and $O(^1S)$ are known, so that correcting for laser power variations and assuming similar ionization efficiencies, we find that the $O(^1S)+N_2(X)$ channel has about 10 ± 1.5 times the quantum yield of the $O(^3P)+N_2(A,B)$ channel. Spin-orbit distributions have also been obtained for all atomic products, and the ratio of quantum yields for the $N(^2D)+NO$ vs. $N(^2P)+NO$ channels is about 3.

---

[1] S. T. Pratt, Ch. Jungen and E. Miescher, J. Chem. Phys. **90**, 5971 (1989).
[2] M. F. Witinski, M. Ortiz-Surez and H. F. Davis, J. Chem. Phys. **122**, 174303 (2005).

G. G. Balint-Kurti and M. P. de Miranda (eds.)
Vector Correlation and Alignment in Chemistry

Imaging atomic orbital polarisation in molecular photodissociation

Claire Vallance,[1] Mark Brouard,[1] Raluca Cireasa,[1] Andrew P. Clark,[1] Fabio Quadrini,[1] Gerrit C. Groenenboom,[2] and Oleg S. Vasyutinskii[3]

[1]*Department of Chemistry, University of Oxford, PTCL, South Parks Rd, Oxford OX1 3QZ, UK*
[2]*Institute for Molecules and Materials, Radboud University Nijmegen, P. O. Box 9010, NL-6500 GL Nijmegen, The Netherlands*
[3]*Ioffe Institute, Russian Academy of Sciences, 94021 St. Petersburg, Russia*

I. INTRODUCTION

Molecular photodissociation studies probe one of the most basic chemical processes, the breaking of a chemical bond. They provide insight into the behaviour of molecules in electronically excited states, and in some cases may also yield information on interactions between different electronic states. Laser pump-probe experiments employing polarised light provide a powerful tool for studying the detailed dynamics of photodissociation, particularly when coupled with state-of-the-art photofragment imaging techniques. In a general pump-probe scheme, reaction is initiated by a pulse of laser light and the photofragments of interest are then interrogated quantum-state selectively using a second laser pulse. In an imaging experiment, the detection step usually consists of ionizing the chosen product quantum state *via* resonance-enhanced multiphoton ionization (REMPI), and employing an electric field to compress the resulting three-dimensional (3D) ion cloud onto a two-dimensional (2D) position sensitive detector. The recorded images represent 2D projections of the 3D photofragment scattering distribution. Aspects of the dissociation dynamics that we are interested in probing include the photofragment speed and angular distributions, and also any photofragment angular momentum polarisation (alignment or orientation) that results from the dynamics of the dissociation process. Measurement of these distributions requires the use of polarised light in both the pump and probe steps.

The speed distribution of the photofragments is determined simply by conservation of energy. For a dissociation $\mathrm{AB} + h\nu \rightarrow \mathrm{A}(v,j) + \mathrm{B}(v,j)$, the available energy is distributed amongst the product translational and internal motion

according to the following energy balance equation:

$$E_{\text{avail}} = h\nu + E_{\text{int}}(\text{AB}) - D_0 = \frac{1}{2}\mu v^2 + E_{\text{int}}(\text{A}) + E_{\text{int}}(\text{B}) \qquad (1)$$

where $h\nu$ is the photon energy, $E_{int}(\text{X})$ is the internal energy of species X, and $\frac{1}{2}\mu v^2$ is the translational kinetic energy of relative motion of the products. The translational kinetic energies K_A and K_B of the two photofragments, and therefore their velocities, may be determined from the total translational energy through straightforward mass relations ($K_\text{A} = [m_\text{B}/(m_\text{A}+m_\text{B})]E_{\text{avail}}$ and $K_\text{B} = [m_\text{A}/(m_\text{A}+m_\text{B})]E_{\text{avail}}$). If both products are atomic, there is generally only a single possible velocity for each fragment, and the images consist of sharp rings. In the more general case, where one or both products are polyatomic, the velocity distribution for one quantum-state-selected photofragment reflects the internal state distribution in the coproduct.

The observed photofragment angular distributions arise from the interaction of the transition dipole $\boldsymbol{\mu}_{\text{phot}}$ for the electronic excitation that leads to dissociation with the polarisation vector $\boldsymbol{\epsilon}_{\text{phot}}$ of the photolysis laser. Only molecules oriented such that there is some overlap between the two vectors are able to absorb light and consequently dissociate. Since the transition dipole lies in a well-defined orientation with respect to the breaking bond, this leads to a strong correlation between the laser polarisation vector and the photofragment velocity. In the extreme cases of a pure parallel or a pure perpendicular transition, the photofragment angular distribution consists of a $\cos^2\theta$ or $\sin^2\theta$ distribution about $\boldsymbol{\epsilon}_{\text{pump}}$. In general, a transition may have both parallel and perpendicular character, and the resulting photofragment angular distribution $I(\cos\theta)$ is given by the well-known expression:

$$I(\cos\theta) = 1 + \beta P_2(\cos\theta) \qquad (2)$$

in which β is a constant with a value between -1 (pure perpendicular transition) and 2 (pure parallel transition) and $P_2(x) = \frac{1}{2}(3x^2 - 1)$ is a second-order Legendre polynomial. The appearance of the images, and their dependence on the photolysis polarisation, therefore provides information about the transition dipole for the initial excitation, and in particular the direction in which it lies relative to the breaking bond. This usually allows the symmetry (and therefore often the identity) of the initially excited state to be determined. It should be noted that the situation is sometimes complicated somewhat by dynamical phenomena such as bending before dissociation, or by the existence of a long-lived excited state that undergoes several rotations before dissociating. In such cases the correlation between $\boldsymbol{\mu}_{\text{pump}}$ and $\boldsymbol{\epsilon}_{\text{pump}}$ is seen to be 'blurred out' to a greater or lesser extent in the images.

The dependence of the images on the polarisation of the *probe* laser is often more subtle, and arises from the fact that the detection efficiency (ionization probability) depends on overlap between the probe laser polarisation $\boldsymbol{\epsilon}_{\text{probe}}$ and

the transition dipole $\boldsymbol{\mu}_{\rm probe}$ for the chosen REMPI transition. Just as the dependence of the images on the photolysis laser polarisation provides information on $\boldsymbol{\mu}_{\rm phot}$, the dependence on the probe laser transition provides information on $\boldsymbol{\mu}_{\rm probe}$. In the former, the transition dipole $\boldsymbol{\mu}_{\rm phot}$ was correlated to the photofragment velocity vector; in the latter, the transition dipole $\boldsymbol{\mu}_{\rm probe}$ is correlated with the *total angular momentum vector* **J** of the probed photofragment (**J** generally lies either parallel or perpendicular to $\boldsymbol{\mu}_{\rm probe}$, depending on the details of the probe transition employed). Any preferential polarisation of **J** leads to a detection sensitivity, and therefore an image, that is sensitive to the probe polarisation. Experimentally measured images may therefore be analysed to determine the angular distribution of **J**.

In polyatomic products, the total angular momentum is dominated by the rotational angular momentum of the fragment, and an anisotropic product angular momentum distribution often provides information on torques acting in the transition state region. For atomic products, the only source of angular momentum is electronic, and an anisotropic angular momentum distribution reflects non-statistical population of M_J (or M_L and M_S) sublevels. The population distributions within these sublevels, and the coherences between them, represent one of the key dynamical properties that may be extracted from the measured images. By considering correlations between the electronic states of the dissociating molecule and the separated photofragments, such information may often be used to infer the symmetry of the dissociating state. This state may or may not be the same as the state initially accessed in the photoexcitation step, depending on whether or not non-adiabatic processes play an important role in the dissociation.

By varying the pump and probe polarisations systematically through a series of 'experimental geometries' and carrying out a thorough and careful analysis of the resulting velocity-map images, it often becomes possible to unravel fairly complicated dissociation pathways in a range of molecular systems.

II. ANALYSING VELOCITY-MAP IMAGES

The photofragment scattering distribution characterises a complete set of vector correlations between the electric vector $\boldsymbol{\epsilon}_{\rm phot}$ of the dissociation light, the transition dipole of the parent molecule $\boldsymbol{\mu}_{\rm phot}$, and the product velocity and angular momentum vectors **v** and **J**. Quantitative extraction of these vector correlations from the experimental data is usually tackled by expanding the scattering distribution in a suitable basis set, usually some variation on a double spherical harmonic expansion in the angles describing the orientations of **v** and **J**, and determining the expansion coefficients using one of a variety of available fitting algorithms. The coefficients constitute a set of 'alignment parameters' that characterise the dynamics of the process under study. The various formalisms for

representing the scattering distribution have resulted in several different sets of alignment parameters being in current use. These include the molecular frame alignment parameters $a_q^k(p)$ proposed by Rakitzis and Zare [1], the alignment anisotropy parameters, $s_2, \alpha_2, \gamma_2, \eta_2$ etc., described by Vasyutinskii, Suits and coworkers [2], and the bipolar moments $b_Q^K(k_1, k_2)$ first described by Dixon [3]. It has been shown that the various formalisms are closely related, and while the physical interpretation of the alignment parameters is somewhat different within each formalism, straightforward expressions exist for transforming between the different sets of parameters [4–6]. The fitted parameters provide all of the information required to reconstruct the product speed and angular distributions, angular momentum polarisation distributions, and M_J state populations. The reader is referred to the extensive literature on the analysis of velocity map images for further details.

III. SYSTEMS STUDIED

Many examples of molecular photodissociation systems exhibiting photofragment polarisation may be found in contributions to this booklet by other authors and in the general scientific literature. The work of the Oxford group, in collaboration with the groups in Nijmegen and St. Petersburg, has focused on probing atomic orbital alignment and orientation in the photofragmentation products of triatomic molecules. The following will provide a brief summary of some of the systems studied to date.

N_2O. Photolysis of N_2O at 193 nm is widely used as a 'clean' source of $O(^1D)$ atoms, and the pathway to $O(^1D)$ production has been well-characterised[7–15]. However, while the major atomic product in the dissociation at this wavelength is $O(^1D)$, a small fraction of the oxygen atoms produced are formed in the $O(^3P)$ ground state, a dissociation pathway that has not previously been studied. There are many potentially interacting, energetically accessible excited state potential energy surfaces, and velocity map imaging provides an ideal tool with which to trace the most likely path from the initially excited electronic state through to the state on which the molecule eventually dissociates. The speed and angular distributions of the atomic products in the $O(^3P)$ channel are similar to those seen for the $O(^1D)$ channel, indicating that the state accessed in the initial excitation is likely to be the same in both cases. The molecular frame M_J disributions resulting from a detailed analysis of the images show some interesting effects. Firstly, for both the $J = 1$ state and the $J = 2$ state, the alignment is fairly small (note that the $J = 0$ state has only one M_J level, so alignment is not possible for this state); and secondly, the alignment has opposite signs for the $J = 1$ and $J = 2$ states i.e. in the $J = 1$ state the levels with larger values of M_J are more highly populated (i.e. **J** lies preferentially *parallel* to **v**), while in the $J = 2$ state the reverse is true (**J** aligned preferentially *perpendicular*

to **v**). These observations may be explained by recourse to a 'fast recoil' model of the dissociation, in which the time scale of the dissociation is much faster than the characteristic time required for spin-orbit coupling to be established between the orbital and spin angular momenta **L** and **S** of the departing atoms. In this limiting case, **L** may be strongly polarised while **S** remains unpolarised. The details of this model are given in reference [16]. The model predicts the correct behaviour of the M_J populations for the $J = 1$ and $J = 2$ spin-orbit states of $O(^3P)$, and also indicates involvement of a state of Σ symmetry in the dissociation. This allows two possible dissociation pathways correlating with $O(^3P)$ products, one proceeding through a Σ state and one through a Π state, to be differentiated.

SO_2. Photodissociation of SO_2 at 193 nm is known to occur *via* the $C\,^1B_2 \leftarrow X\,^1A_1$ electronic transition and to yield electronic ground state $O(^3P)+SO(^3\Sigma^-)$ products [17, 18]. The initially populated excited state correlates with a product channel, $O(^1D) + SO(^1\Delta)$ [18], that is energetically inaccessible at this wavelength. Dissociation must therefore occur via nonadiabatic transfer onto one or more of the electronic surfaces asymptotically correlating with the ground state product channel. Previous studies of this system have proposed three distinct mechanistic pathways: an internal conversion of excited state population back onto quasi-bound continuum levels of the ground electronic state [18–20]; an intersystem crossing onto a repulsive triplet surface [21, 22]; and an avoided crossing with a repulsive singlet surface [23, 24].

The electronic angular momentum alignment of the $O(^3P)$ product has been quantified, using the velocity map imaging technique, with a view to distinguishing between the various possible dissociation pathways [25]. The data show qualitatively similar trends to those observed for N_2O, with the alignment of **J** again opposite in sign for the $J = 1$ and $J = 2$ states; however, the 'fast dissociation' model is not applicable in this case since the excited-state SO_2 is known to have a fairly long lifetime before dissociation. A model has been developed that incorporates the possibility of polarisation not only of the orbital angular momentum, but also of the O-atom electron spin. Data analysis suggests that both **L** and **S** are aligned in this system, perpendicular both to one another and to the recoil direction. Long range potentials modelling the dipole-quadrupole or quadrupole-quadrupole interactions between the fragments as a function of bending angle have also been developed. These calculations suggest that product alignment will depend sensitively on bending motions in the dissociating molecule. The study does provide some qualitative support for the internal conversion mechanism, but it is important to emphasise that a full dynamical treatment, taking into account averaging over the bending angle, would be necessary to obtain a quantitative comparison between experimental and theoretical results.

Current studies. More recently, similar experimental studies imaging the $O(^3P)$ products from NO_2 photolysis at 308 nm [26] and the $O(^1D)$ products from O_3 photodissociation at 193 nm [27] have been undertaken. Interestingly,

preliminary results suggest negligible atomic angular momentum alignment in the former case, but very strong polarisation in the latter.

IV. CONCLUSIONS

Polarised laser pump-probe techniques coupled with velocity map imaging of the product scattering distribution are effective tools for the investigation of energetic and dynamical effects in chemical systems. Supported by continuing advances in the theory underlying the measurement and interpretation of atomic and molecular polarisation effects, these techniques are providing ever more detailed insights into the basic physics underlying a variety of unimolecular and bimolecular processes.

Acknowledgements. We thank the EPSRC and the Royal Society for funding.

---

[1] T. P. Rakitzis and R. N. Zare, J. Chem. Phys. **110**, 3341 (1999).
[2] A. S. Bracker, E. R. Wouters, A. G. Suits and O. S. Vasyutinskii, J. Chem. Phys **110**, 6749 (1999).
[3] R. N. Dixon, J. Chem. Phys. **85**, 1866 (1986).
[4] B. V. Picheyev, A. G. Smolin and O. S. Vasyutinskii, J. Phys. Chem. A **101**, 7614 (1997).
[5] T. P. Rakitzis, G. E. Hall, M. L. Costen and Zare RN, J. Chem. Phys. **111**, 8751 (1999).
[6] M. J. Bass, M. Brouard, A. P. Clark, C. Vallance and B. Martinez-Haya, Phys. Chem. Chem. Phys. **5**, 856 (2003).
[7] P. Felder, B.-M. Haas and J. R. Huber, Chem. Phys. Lett. **186**, 177 (1991).
[8] N. Shafer, K. Tonokura, Y. Matsumi, S. Tasaki and M. Kawasaki, J. Chem. Phys. **95**, 6218 (1991).
[9] L. L. Springsteen, S. Satyapal, Y. Matsumi, L. M. Dobeck and P. L. Houston, J. Phys. Chem. **97**, 7239 (1993).
[10] T. Suzuki, H. Katayanagi, Y. Mo and K. Tonokura, Chem. Phys. Lett. **256**, 90 (1996).
[11] Y. Matsumi and A. M. S. Chowdhury, J. Chem. Phys. **104**, 7036 (1996).
[12] D. W. Neyer, A. J. R. Heck, D. W. Chandler, J. M. Teule and M. H. M. Janssen, J. Phys. Chem. A **103**, 10388 (1999).
[13] D. W. Neyer, A. J. R. Heck, D. W. Chandler, J. Chem. Phys. **110**, 3411 (1999).
[14] M. Ahmed, E. R. Wouters, D. S. Peterka, O. S. Vasyutinskii and A. G. Suits, Faraday Discuss. Chem. Soc. **113**, 425 (1999).
[15] J. M. Teule, G. C. Groenenboom, D. W. Neyer, D. W. Chandler and M. H. M. Janssen, Chem. Phys. Lett. **320**, 177 (2000).
[16] M. Brouard, A. P. Clark, C. Vallance and O. S. Vastyutinskii, J. Chem. Phys. **119**,771 (2003).
[17] H. Okabe, J. Am. Chem. Soc. **93**, 7095 (1971).

[18] H. Katagiri, T. Sako, A. Hishikawa, T. Yazaki, K. Onda, K. Yamanouchi and K. Yoshino, J. Mol. Struct. **413-414**, 589 (1997).
[19] M. Ivanco, J. Hager, W. Sharfin and S. Wallace, J. Chem. Phys. **78**, 6531 (1983).
[20] A. Okazaki, T. Ebata and N. Mikami, J. Chem. Phys. **107**, 8752 (1997).
[21] T. Ebata, O. Nakazawa and M. Ito, Chem. Phys. Lett. **143**, 31 (1998).
[22] H. Kanamori, J. E. Butler, K. Kawaguchi, C. Yamada and E. Hirota, J. Chem. Phys. **83**, 611 (1985).
[23] Y. Tzyy-Schiuan and A. B. Myers, J. Chem. Phys. **95**, 6207 (1991).
[24] P. C. Ray, M. F. Arendt and L. J. Butler, J. Chem. Phys. **109**, 5221 (1998).
[25] M. Brouard, R. Cireasa, A. P. Clark, G. C. Groenenboom, T. J. Preston, C. Vallance and O. S. Vasyutinksii, J. Phys. Chem. A **108**, 7965 (2004).
[26] M. Brouard, R. Cireasa, A. P. Clark, T. J. Preston and C. Vallance, work in progress.
[27] M. Brouard, R. Cireasa, A. P. Clark, G. Hancock, S. Horrocks, G. Ritchie and C. Vallance, work in progress.

G. G. Balint-Kurti and M. P. de Miranda (eds.)
Vector Correlation and Alignment in Chemistry

Stereo-chemical and correlation effects in photodissociation

Richard N. Dixon
School of Chemistry, University of Bristol, BS8 1TS, UK

I. INTRODUCTION

Molecular dissociation is a primary chemical process in which the initial parent state can be closely defined, and it has therefore attracted much experimental and theoretical interest. The dynamics of a photodissociation process depend on the geometry, potential functions, and lifetimes of the excited states of the parent molecule, together with any intramolecular redistribution or exit-channel interactions which may influence the motion of the recoiling fragments. Excitation with polarised laser beams usually generates an anisotropic ensemble of excited molecules, thereby revealing vector correlations that provide a powerful characterisation both of the excitation step and of the dissociation dynamics. In principle the excitation and subsequent dynamics form a single correlated process, coupling the initial state to an outgoing scattering wave for the fragments which is itself a correlated function of their centre of mass recoil wave vector and of their internal motion. However, in many cases and particularly with nanosecond laser sources, it is informative to consider separate steps of excitation, initial fragment recoil, and exit channel re-arrangements.

II. SINGLE PHOTON DISSOCIATION

The theory for single photon dissociation is well developed and extensively implemented. Dipole excitation with linearly polarised light of an isotropic sample of molecules, even when these are all in a single rotational state, leads to the space-fixed distribution function

$$P(\theta_R) = \left[1 + \beta P_2(\cos\theta_R)\right]/4\pi \tag{1}$$

where θ_R is the angle between the recoil vector $\mathbf{R}$ and the electric vector $\boldsymbol{\varepsilon}$ of the radiation, and P_2 is a Legendre polynomial. Many measurements of this type have involved excitation within a continuum or quasi-continuum, so that the molecule dissociates rapidly on the time scale of molecular rotation. For

those polyatomic molecules, in which rapid dissociative recoil may take place in the body-fixed frame at some range of angles to the dipole axis, the anisotropy parameter is given by the ensemble average:

$$\beta = 2\big\langle P_2(\mathbf{R}\cdot\boldsymbol{\mu})\big\rangle, \qquad -1 \le \beta \le 2 \tag{2}$$

where $\boldsymbol{\mu}$ is the transition dipole. In contrast, for a long-lived parent excited state its spatial anisotropy often depends on rotational quantum numbers because of the precession of $\boldsymbol{\mu}$ about $\mathbf{J}'$, and this variation is reflected in β.

The anisotropy of excitation may also result in an anisotropy of the rotational angular momentum distribution of molecular fragments. Possible correlations between the directions of fragment recoil and rotation [1] can be extracted from the Doppler profiles of LIF spectra or ion time-of-flight spectra, using a range of excitation-detection geometries, or velocity map imaging. In particular, a positive value of the correlation moment $\beta^0_0(2\,2)$ indicates a tendency of $\mathbf{v}_f$ and $\mathbf{J}_f$ to be parallel (propeller motion as in H_2O_2 [2]), but perpendicular for a negative value (cartwheel motion).

We will illustrate this theory with three of the more unusual findings.

(a) It is usually assumed that dissociation of a diatomic molecule via a repulsive potential takes place along the bond axis. However this axial recoil approximation has been noted to break down for excitation of IBr and of Br_2 at energies very close to the dissociation threshold. Then, even in a jet-cooled molecular beam, the time-scale of parent rotation is comparable with that of recoil beyond the molecular potential, leading to a degradation of β from its limiting value that increases with J [3].

(b) In general, β gives the projection of $\mathbf{R}$ onto a unique molecular axis. But in the case of predissociation of HFCO, via its $\tilde{A}\,{}^1A''$ state, it has been possible to determine separate values of β for the asymmetric top transitions ${}^rR(0)$, ${}^rR(1)$ and ${}^pQ(\text{all } J)$, giving projections of β onto all three inertial axes [4]. This leads to average values for both of the body-fixed polar angles of recoil, thereby providing strong evidence that the predissociation is mediated by intersystem crossing to the lowest triplet state ($\tilde{a}\,{}^3A''$).

(c) The recoil anisotropy of H-atoms, resulting from the dissociation of NH_3 through the lowest ($v_2 = 0\,\&\,1$) partially structured vibrational levels of the planar first excited ($\tilde{A}\,{}^1A_2$) singlet state, varies widely with the internal energy of the NH_2 partner fragment, with β ranging from $+1.4$ to -0.9. These data are accurately modelled by taking account of two new factors: (i) the parent spatial anisotropy includes contributions from partial coherence of overlapping rotational transitions; and (ii) the product angular momentum is generated by internal conversion at a conical intersection at $R_{\rm NH} = 1.96\,\text{Å}$ of the excited and ground state potentials. Consequently for low internal energy the H-atom departs in the molecular plane and thus perpendicular to the top axis ($\beta \to -1$), but the balancing of high angular momentum requires departure perpendicular to this plane ($\beta \to +2$) [5].

III. MULTIPHOTON DISSOCIATION

Multiphoton excitation is increasingly used to access the higher molecular electronic states, often combined with the use of near resonant intermediate states to enhance the dissociation yield. This inevitably leads to higher order distribution laws that now depend on the orbital properties of all the states involved. Furthermore, partial rotation at an intermediate stage can lead to further complication, even if the final state dissociates rapidly on the time-scale of molecular rotation. In the limit that such an intermediate state has a lifetime long compared with rotation, this offers the possibility of excitation via a single intermediate rotational state. The anisotropy of the ensemble of transiently populated states is then dependent not only on the directions of the transition moments in a body-fixed frame, but also on the rotational transition for excitation. Similar consequences arise if the final excited state is rotationally structured.

The advent of velocity map imaging methods for investigating quantum state resolved photodissociation has greatly enhanced the ease and precision of measurement of recoil anisotropy distributions. Recent measurements of the H atom photofragment angular distributions from two-photon excitation of HCl and HBr provide a detailed example of this process. Two-photon Q-branch excitation to the rotationally structured $E\,^1\Sigma^+$ state of HCl, and the $H\,^1\Sigma^+$ state of HBr, was used as an intermediate step, followed by single photon dissociation via continua. A formalism was also developed for such a process involving a J-selected intermediate state, leading to the identity of the virtual intermediate state to the two-photon step and the symmetry of the dissociative state [6].

The process of multi-photon excitation involves the simultaneous absorption by a molecule of several photons such that the sum of their energies is in resonance with a transition from an initial state $|1\rangle$ to a final state $|2\rangle$. Within this framework the molecule reaches the final state via one or more virtual intermediate states $|v_i\rangle$. These virtual states represent the molecule dressed with one or more photons, and can each be expanded in terms of the complete basis of real states $|j\rangle$, $|k\rangle$, *etc.* In the limit that all such real intermediate states are either far from resonance, or have lifetimes which are very short compared with the time-scale of parent rotation, the angular distribution of excitation to the final state can be described in terms of N-photon transition tensors, each of which is independent of rotational quantum numbers and satisfies the molecular symmetry rule:

$$\Gamma\big((T^k_q(\mu^N)\big) \subset \Gamma(\Psi_1) \otimes \Gamma(\Psi_2), \qquad k = N, N-2 \ \textit{etc.} \tag{3}$$

This rule is well understood for determining the structure of two- and three-photon multi-photon excitation spectra, and has been invoked in the analyses of countless such spectra.

Table 1 lists the sets of transition tensors for 2- and 3-photon excitation of a

N	Λ_1, Λ_2	$T_q^k(\mu^N)$	N	Λ_1, Λ_2	$T_q^k(\mu^N)$
2	$0,0$	T_0^0, T_0^2	3	$0,0$	T_0^1, T_0^3
	$0,1;\ 1,0$	$T_{\pm1}^2$		$0,1;\ 1,0$	$T_{\pm1}^1, T_{\pm1}^3$
	$0,2;\ 2,0$	$T_{\pm2}^2$		$0,2;\ 2,0$	$T_{\pm2}^3$
	$1,1$	$T_0^0, T_0^2, T_{\pm2}^2$		$0,3;\ 3,0$	$T_{\pm3}^3$
	$1,2;\ 2,1$	$T_{\pm1}^2$		$1,1$	$T_0^1, T_0^3, T_{\pm2}^3$
	$1,3;\ 3,1$	$T_{\pm2}^2$		$1,2;\ 2,1$	$T_{\pm1}^1, T_{\pm1}^3, T_{\pm3}^3$
	$2,2$	T_0^0, T_0^2		$1,3;\ 3,1$	$T_{\pm2}^3$
	$2,3;\ 3,2$	$T_{\pm1}^2$		$2,2$	T_0^1, T_0^3
				$2,3;\ 3,2$	$T_{\pm1}^1, T_{\pm1}^3$
				$3,3$	T_0^1, T_0^3

TABLE I: Allowed N-photon spherical tensors.

linear molecule from a state with axial quantum number Λ_1 to a final state Λ_2. (The same theory will apply to Hund's cases (a) or (c) by replacing Λ by Ω, or by K for a polyatomic symmetric top molecule.)

Many experiments using multi-photon excitation exploit the enhancement given by real states lying close to the virtual states. In such cases the transition probability may be dominated by the contribution from a single real excitation pathway, with the consequence that the set of tensors of Table 1 becomes restricted to a uniquely defined transition tensor. We will use such individual pathways as the basis of discussion. In evaluating the elementary transition moments μ_{kj} for each single-photon step the molecular-axis transition tensors $T_q^k(\mu)$ ($k = 1$ for dipole transitions) must be expressed in the space-fixed axis system:

$$T_q^k(\mu) = \sum_p T_p^k(\mu) D_{pq}^k(\omega)^*. \tag{4}$$

The transformation of the N-photon product of single- photon tensors $T_q^k(\mu)$ to the space-fixed frame therefore requires a product of rotation matrices, which product can be re-expressed as a linear combination with coefficients C_{KPQ}:

$$\prod_{1=1}^{N} D_{pq_i}^1(\omega)^* = \sum_K \sum_Q C_{KPQ} D_{PQ}^K(\omega)^*. \tag{5}$$

where $P = Np$ and $Q = \Delta\Lambda$ (capitals for multi-photon quantum numbers).

Thus excitation from the initial state can lead to upper states with $\Delta\Lambda \leq N$, noting in this respect that Λ must be treated as a signed quantum number. In all cases the possible values of K and Q are restricted to those contained within Table 1.

In all cases of multi-photon excitation from an isotropic ensemble of initial state molecules, eq. (1) is replaced by:

$$P(\theta) = \left[1 + \sum_{n\geq 2}^{2N} \beta_n P_n(\cos\theta)\right]/4\pi \tag{6}$$

where the moments of this ensemble are denoted by β_n, and n is restricted to $n \leq 2N$. We seek to relate these moments to the products of eq. (5).

A. Dissociation without rotation

Rotation in an intermediate state can be neglected if either (a) the lifetime of the intermediate state is sufficiently short that its homogeneous line-width Γ is much greater than its rotational spacings, or (b) the state is sufficiently off-resonant that the various energy offsets Δ_j for a given J are all approximately equal. If the final excited state also decays rapidly compared with the time-scale of parent rotation, then the coherence of the various final ro-vibronic states will not be significantly dephased during dissociation. Furthermore, most experiments are carried out on isotropic ensembles of initial state molecules. The corresponding spatial anisotropic moments of the excited state are then related to the transition tensors by:

$$\beta_n = [n]\frac{\sum_{K_i}\sum_{K_j}\sum_Q (-1)^{P-Q} C_{K_i PQ} C_{K_j PQ} \begin{pmatrix} K_i & K_j & n \\ P & -P & 0 \end{pmatrix} \begin{pmatrix} K_i & K_j & n \\ Q & -Q & 0 \end{pmatrix}}{\sum_K \sum_Q C^2_{KPQ}/[K]} \tag{7}$$

which reduces if there is either only one, or one degenerate pair, of transition tensors to:

$$\beta_n = (-1)^{P-Q}[n]\,[k] \begin{pmatrix} K & K & n \\ P & -P & 0 \end{pmatrix} \begin{pmatrix} K & K & n \\ Q & -Q & 0 \end{pmatrix} \tag{8}$$

where $[x] = 2x + 1$, and $\begin{pmatrix} \cdots \\ \cdots \end{pmatrix}$ is a $3j$ symbol. This is the N-photon generalisation of the well-known one-photon equation. Dissociation along the top axis will result in a product recoil anisotropy equal to this spatial anisotropy for the excited state. However, for those polyatomic molecules in which rapid dissociative recoil may take place in the body-fixed frame at some range of angles γ to the top axis, each moment β_n will be degraded by multiplication by the ensemble average $\langle P_n(\cos\gamma)\rangle$.

B. Multiple excitation pathways

Multiple excitation pathways require multiple products of transition tensors. These may occur either through contributions from several real intermediate states, or because there is more than one accessible final state at the multi-photon energy dissociating to the same products. In many cases with several tensor products the anisotropy is sensitive not only to the relative amplitudes of the multiple pathways, but also to their relative phases.

Consider, for example, the two-photon pathways $\Sigma \rightarrow \Sigma \rightarrow \Sigma$ and $\Sigma \rightarrow \Pi \rightarrow \Sigma$ in linear polarisation. $P(\theta)$ is proportional to the square of the sum of the two transition tensors, which are individually proportional to $\cos^2\theta$ ($\beta_2 = +20/7$; $\beta_4 = +8/7$) and $\sin^2\theta$ ($\beta_2 = -10/7$; $\beta_4 = +3/7$) respectively. Should these contribute with equal amplitude and sign, as might occur with near degenerate $np\sigma$ and $np\pi$ Rydberg states as intermediates, then the resultant tensor will be independent of θ, and both β_2 and β_4 will be zero. In contrast, with equal but opposite amplitudes, the sum is proportional to $\cos(2\theta)$, and thus $P(\theta) = \cos^2(2\theta)$ with moments $\beta_2 = -40/49$ and $\beta_4 = +96/49$. However, in circular polarisation $P(\theta) = \sin^4(\theta)$ for both these pathways and the resultant is therefore independent of their relative contributions. Thus, if it is known that a two-photon transition to a short-lived state is overall $\Sigma \rightarrow\!\!\!\rightarrow \Sigma$, then the relative amplitude *and phase* of these two pathways can be deduced from measurements of the recoil anisotropy in linear polarisation, but not from circular polarisation.

C. Pre-dissociation of the final state or an intermediate state

Pre-dissociation of the final excited state on a time-scale such that the homogeneous line-width Γ is comparable with rotational spacings will result in a partial dephasing of the coherent super-position of ro-vibronic states. In the near limiting case that $\Gamma \gg BJ$, and thus any rotational structure is completely lost within the line broadening, it is appropriate to use a quasi-classical approach. The top axis of the rotating molecule will continue to rotate while the excited population decays exponentially in time into recoiling products. The consequence is an exponentially decaying distribution of post excitation rotation angles γ, with a ratio of angular frequency to time decay constant which equates to $2B|\mathbf{J}|/\Gamma$, where $|\mathbf{J}| = \sqrt{J(J+1) - \Lambda^2}$. Each excitation moment of the nascent anisotropy will become attenuated by multiplication by $\langle P_n(\cos\gamma)\rangle$.

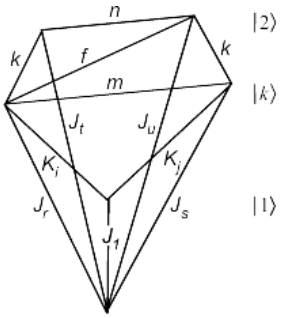

FIG. 1: The angular momentum coupling scheme via an intermediate state. J_1 relates to state $|1\rangle$, J_r and J_s to state $|k\rangle$, and J_t and J_u to state $|2\rangle$. β_m & β_n are recoil moments.

Evaluation of these expectation values, normalised to $\langle P_0(\cos\gamma)\rangle = 1$, leads to:

$$\langle P_2(\cos\gamma)\rangle = \frac{1}{4}\left(\frac{3}{4x^2+1}+1\right), \tag{9a}$$

$$\langle P_4(\cos\gamma)\rangle = \frac{1}{64}\left(\frac{35}{16x^2+1}+\frac{20}{4x^2+1}+9\right), \tag{9b}$$

$$\langle P_6(\cos\gamma)\rangle = \frac{1}{512}\left(\frac{231}{36x^2+1}+\frac{126}{16x^2+1}+\frac{105}{4x^2+1}+50\right), \tag{9c}$$

where $x = 2B|\mathbf{J}|/\Gamma$. Thus limited rotation leads to increasing degradation of the moments as n increases, as might have been expected from the nodal structures of the $P_n(\cos\gamma)$ functions. One consequence of this is that any peaks in the anisotropy distribution will tend to move towards $\theta = 0$ or $\pi/2$, depending on the sign of β_2. For the case where $x > 0.5$, such that the spacings between rotational transitions for a given J exceed the line half-widths ($2BJ > \Gamma/2$), or for the extreme case with $BJ \gg \Gamma$ but with a lack of resolution because of rotational congestion, the anisotropy will vary across the excitation spectrum.

In carrying out multi-photon dissociation it is common to make use of the enhancement provided by any real states that lie close to the virtual states. Partial rotation in such an intermediate state can again be expected to influence the recoil anisotropy, even when the final state is very short lived. In such a case the transition tensors of the two steps cannot be contracted as in eq. (5), but must be considered separately. The first step sets up a transient anisotropy in the intermediate state $|k\rangle$ with moments β_m; but these will become degraded by partial rotation through the loss of coherence of J_r with J_s at this stage (see Fig. 1). The final state anisotropy is then a convolution of this degraded intermediate anisotropy with that from the final excitation step. Each final

moment β_n has contributions from the intermediate moments β_m, where $|m - n| \leq 2k$.

This discussion has concentrated on the excitation steps. The subsequent recoil for polyatomic parent molecules may be influenced by exit-channel effects, and by correlations with fragment rotation, as for single-photon dissociation.

IV. CONCLUSION

This paper has shown that the anisotropy of recoiling fragments following multi-photon dissociation can provide detailed information on the symmetries of the various states involved, including possible interference between multiple pathways. The comparison between the recoil anisotropies recorded using linear and circular polarisation schemes can assist with this.

Where there is significant rotation of the parent molecule before fragmentation the clear distinctions between the various pathways can be severely eroded, although completely resolved excitation represents another well-defined limiting case. The full theory of the influence of parent rotation on recoil anisotropy is given in detail in a recent paper [7].

[1] R. N. Dixon, J. Chem. Phys. **85**, 1866 (1986).
[2] K. H. Gericke, S. Klee, F. J. Comes and R. N. Dixon, J. Chem. Phys. **85**, 4463 (1986).
[3] E. Wrede, E. R. Wouters, M. Beckert, R. N. Dixon and M. N. R. Ashfold, J. Chem. Phys. **116**, 6064 (2002).
[4] R. N. Dixon and T. W. R. Hancock, J. Phys. Chem. **101**, 7567 (1997).
[5] D. H. Mordaunt, M. N. R. Ashfold and R. N. Dixon, J. Chem. Phys. **104**, 6460 (1996).
[6] S. Manzhos, C. Romanescu, H-P. Loock and J. G. Underwood, J. Chem. Phys. **121**, 11802 (2004).
[7] R. N. Dixon, J. Chem. Phys. **122**, 194302 (2005).

G. G. Balint-Kurti and M. P. de Miranda (eds.)
Vector Correlation and Alignment in Chemistry

Electrostatic long range effects on photofragment polarization

Gerrit C. Groenenboom
Institute of Theoretical Chemistry, IMM, University of Nijmegen, Toernooiveld 1, 6525 ED Nijmegen, The Netherlands

I. INTRODUCTION

Detailed information about a photodissociation process can be obtained by studying the spatial distribution and the polarization of the photofragments. Experimental techniques for this purpose are velocity mapped ion imaging[1], time of flight mass spectrometry [2–4], and fast beam photo-fragment spectroscopy [5]. The quantum mechanical theory for the photodissociation of diatomic molecules to atoms with nonvanishing electronic angular momentum was presented by Singer *et al.*[6]. A quantum treatment of the correlation between the spatial anisotropy and the angular momentum polarization of the fragments was given by Siebbeles *et al.*[7]. To gain insight into the photodissociation mechanism it is worthwhile to study the low and high excess kinetic energy limits of a simplified model of the process. For the dissociation of a diatomic molecule where one photofragment is produced in an S-state adiabatic (low energy) and diabatic (high energy) models can be constructed which only depend on the symmetry of the molecular states involved in the dissociation. In this mini-review I will also discuss how photodissociation involving two open-shell, i.e., two non S-state fragments and triatomic systems can be treated analytically by considering the electrostatic long range effects. The methods discussed here have been applied to the photodissociation of O_2[4, 8], O_2^-[5], N_2O[9], SO_2[10].

II. ONE OPEN-SHELL FRAGMENT

First consider the direct dissociation of a diatomic molecule into an S-state atom A and an open-shell atom B with total orbital angular momentum L_B through a single intermediate state

$$\mathrm{AB} + h\nu \rightarrow \mathrm{AB}(\Lambda) \rightarrow \mathrm{A}(S) + \mathrm{B}(L_B\Lambda_B). \tag{1}$$

In this case the projection of the orbital angular momentum onto the interatomic axis (Λ) is preserved by the open-shell atom, i.e., $\Lambda_B = \Lambda$, if we may neglect the coupling to overall rotation and to nuclear or electronic spin. If the open-shell atom B has non-zero electron spin the atomic fine-structure states are characterized by the total angular momentum J_B and its projection Ω_B arising from the coupling of orbital and spin angular momenta (S_B and projection Σ_B)

$$|(L_B S_B) J_B \Omega_B\rangle = \sum_{\Lambda_B \Sigma_B} |L_B \Lambda_B\rangle |S_B \Sigma_B\rangle \langle L_B \Lambda_B S_B \Sigma_B | J_B \Omega_B\rangle, \qquad (2)$$

where $\langle \cdots | \cdots \rangle$ is a Clebsch-Gordan coefficient. When the recoil velocity is small compared to the spin-orbit coupling a (spin-orbit) *adiabatic* model applies: a single fine-structure level J_B will be populated, which can be determined from a correlation diagram in which $\Omega = \Lambda + \Sigma$ is a good quantum number, with Σ the projection on the interatomic axis of the molecular spin S. With atom A in a ^1S state the polarization of atom B follows from $\Omega_B = \Omega$, where the population of the Ω levels is determined in the excitation step.

For recoil kinetic energies much larger than the spin-orbit coupling the *diabatic* model applies. In this case it is assumed that the molecular state $|S\Sigma\Lambda\rangle$ gives rise to an atomic state with $\Lambda_B = \Lambda$ and $\Sigma_B = \Sigma$. The fine-structure branching ratios and fragment polarization can now be obtained from the inverse of Eq. (2).

III. TWO OPEN-SHELL FRAGMENTS

We now consider a photodissociation reaction producing two open-shell fragments

$$\mathrm{AB} + h\nu \rightarrow \mathrm{AB}(\Lambda) \rightarrow \mathrm{A}(^{2S_A+1}L_A) + \mathrm{B}(^{2S_B+1}L_B). \qquad (3)$$

If we again ignore the spin-orbit coupling we find $\Lambda_A + \Lambda_B = \Lambda$, which in general is not sufficient to determine the orbital polarizations of the fragments. Several *adiabatic Born-Oppenheimer* molecular states of the same symmetry ($|n\Lambda\rangle$) will correlate with the $|L_A L_B\rangle$ asymptote. For large internuclear separations the molecular states $|n\Lambda\rangle$ may be expressed as linear combinations of the product atomic states $|L_A \Lambda_A\rangle |L_B \Lambda_B\rangle$ with $\Lambda_A + \Lambda_B = \Lambda$. The proper linear combinations may be found by diagonalization of the leading interatomic term of the multipole expansion of the Coulomb interaction in the $|L_A \Lambda_A\rangle |L_B \Lambda_B\rangle$ basis. For example, taking into account the charge-quadrupole interaction in the photodissociation $O_2^- \rightarrow O^-(^2P) + O(^3P)$ it is found that the lowest Π state corresponds to $|10\rangle|11\rangle$ and the second to $|11\rangle|10\rangle$ [5]. For the dissociation of O_2 into $O(^3P)$+$O(^3P)$ it turns out that asymptotically the $A^3\Sigma_u^+$ and the $2^3\Sigma_u^+$ states correspond to the coupled atomic states $\sum_{\Lambda_A \Lambda_B} |1\Lambda_A 1\Lambda_B\rangle \langle 1\Lambda_A 1\Lambda_B | L0\rangle$

with $L = 0$ and $L = 2$, respectively [11]. The spin part of the wave function is found from Clebsch-Gordan coupling of the atomic spin-functions to the molecular spin $|(S_A S_B)S\Sigma\rangle = \sum_{\Sigma_A \Sigma_B} |S_A \Sigma_A\rangle |S_B \Sigma_B\rangle \langle S_A \Sigma_A S_B \Sigma_B | S\Sigma\rangle$. Fine-structure branching ratios and fragment polarization in the spin-orbit diabatic model are obtain by expanding the product of the orbital and spin wave functions in product atomic fine-structure functions $|J_A \Omega_A\rangle |J_B \Omega_B\rangle$. However, the same symmetry molecular states $|n\Lambda\rangle$ are also coupled by the nonadiabatic radial derivative coupling, which must be taken into account in the high energy limit. For the photodissociation of O_2 through the $A(^2\Sigma_u^+)$ state it was shown by integrating the radial derivative coupling obtained from *ab initio* calculations that the $2^2\Sigma_u^+$ state may reach a 30% population in the high enery limit [8].

In the spin-orbit adiabatic limit a correlation diagram using $\Omega = \Omega_A + \Omega_B$ as a good quantum number can be used. To determine the linear combinations of the $|j_A \Omega_A\rangle |j_B \Omega_B\rangle$ product atomic states that correspond to the spin-orbit adiabatic states we must again consider the long-range electrostatic interactions. Even for dissociation just above threshold the kinetic energy available due to the electronic interaction may be sufficient to induce nonadiabatic transitions between states with the same Ω and the low energy spin-orbit adiabatic limit may never be reached.

IV. TRIATOMIC SYSTEMS

The models presented to describe the photodissociation of diatomic molecules can be extended to ABC+$h\nu \rightarrow$ AB+C photodissociation. A new feature is that the long range electrostatic interaction, which must again be considered to define adiabatic models, will depend on the Jacobi angle θ between the diatomic axis (AB) and the center of mass vector AB—C. However, in general the AB fragment will be rotating and the angle θ will not reach an asymptotic value, but instead—in a classical description of the nuclear motion—it will be a function of the center of mass separation (R) of the fragments. At a certain distance R the atom-diatom interaction will be sufficiently weak for the atomic polarization in the lab-fixed space to reach its asymptotic value. At this point the adiabatic model must break down. In the short range the separation between the electronic states is typically large and an adiabatic description can generally be expected to be valid. Hence, to apply the adiabatic model a critical distance R and Jacobi angle θ must be chosen at which the electrostatic interaction matrix is computed. Since the critical geometry will not be known without a dynamical calculation the predictive power of the model is limited, but since it is very simple to work out the model for the full range of angles and the dependence on the distance R is weak, it is still useful for a qualitative analysis of the data. So far this model has been applied to $N_2O+h\nu \rightarrow N_2 + O(^1D)$ [9] and to $SO_2 + h\nu \rightarrow SO(^3\Sigma^-) + O(^3P)$ [10].

V. CONCLUSION AND OUTLOOK

The application of the adiabatic and diabatic models to diatomic molecules is straightforward. When experimental photofragment data is not described by either model it can be expected to provide a stringent test of more advanced theoretical models of the dissociation process. For several diatomic systems full quantum descriptions of the dissociation process have been compared to experimental data. For triatomic systems the validity of an adiabatic model based on a critical geometry has yet to be tested by more advanced theories.

In recent years many techniques have been developed to cool molecules to the 1K regime. The cold molecules can be trapped and manipulated by electric and magnetic fields. These new techniques provide the prospect of detailed study of interacting open-shell species and photodissociation experiments for trapped molecules are planned. In the low energy regime resonances are expected to result in deviation from simple adiabatic behavior.

---

[1] A. T. J. B. Eppink and D. H. Parker, Rev. Sci. Instrum. **68**, 3477 (1997).
[2] T. P. Rakitzis and R. N. Zare, J. Chem. Phys. **110**, 3341 (1999).
[3] T. P. Rakitzis, S. A. Kandel, A. J. Alexander, Z. H. Kim and R. N. Zare, J. Chem. Phys. **110**, 3351 (1999).
[4] A. J. Alexander, Z. H. Kim and R. N. Zare, J. Chem. Phys. **118**, 10566 (2003).
[5] L. Dinu, G. C. Groenenboom and W. J. van der Zande, J. Chem. Phys. **119**, 8864 (2003).
[6] S. J. Singer, K. F. Freed and Y. B. Band, J. Chem. Phys. **79**, 6060 (1983).
[7] L. D. A. Siebbeles, M. Glass-Maujean, O. S. Vasyutinskii, J. A. Beswick and O. Roncero, J. Chem. Phys. **100**, 3610 (1994).
[8] M. C. G. N. van Vroonhoven and G. C. Groenenboom, J. Chem. Phys. **116**, 1965 (2002).
[9] J. M. Teule, G. C. Groenenboom, D. W. Neyer, D. W. Chandler and M. H. M. Janssen, Chem. Phys. Lett. **320**, 177 (2000).
[10] M. Brouard, R. Cireasa, A. P. Clark, T. J. Preston, C. Vallance, G. C. Groenenboom and O. S. Vasyutinskii, J. Phys. Chem. A **108**, 7965 (2004).
[11] M. C. G. N. van Vroonhoven and G. C. Groenenboom, J. Chem. Phys. **116**, 1954 (2002).

G. G. Balint-Kurti and M. P. de Miranda (eds.)
Vector Correlation and Alignment in Chemistry

Orientation and alignment of $O(^1D_2)$ in the UV photodissociation of ozone

Suk Kyoung Lee,[1,2] Dave Townsend,[3] and Arthur G. Suits[1,2]

[1] *Department of Chemistry, Wayne State University, Detroit MI 48202, USA*
[2] *Department of Chemistry, Stony Brook University, Stony Brook, NY 11794, USA*
[3] *Steacie Institute for Molecular Sciences, National Research Council of Canada, Ottawa, ON, K1A 0R6, Canada*

It has long been known that photofragments produced by photodissociation with polarized light can be aligned or oriented. Recently, the recoil angle dependence of orbital polarization has become the focus of study rather than the total net angular momentum polarization owing to the fact that the former can give us the dynamical information in the molecular frame [1].

The angular momentum polarization can be conveniently expanded in terms of multipole moments, ρ_{KQ} of rank K and component Q. The zeroth order multipole moment corresponds to the photofragment differential cross section, while odd and even order multipole moments describe the orientation and alignment, respectively. These polarization effects are directly manifested in nonequilibrium populations of magnetic sublevels m_J, which, in the axial recoil approximation, are projections of the total angular momentum J onto the bond-breaking axis. In general, rank $K = 1$ and 2 are considered as major contributions to orientation and alignment, respectively, even though higher rank multipoles up to $K = 2J$ exist and should be included for a complete analysis. However, the higher order terms can be neglected by selecting a suitable probe scheme which is sensitive only to the contribution to total angular momentum polarization from a given rank multipole moment.

Our group recently developed the DC slice imaging technique, which is a powerful method to investigate the speed-dependent orbital polarization for any system, as a narrow central section of three-dimensional (3D) ion sphere can be directly measured without need for any reconstruction, and crossed laser polarization geometries may be employed [2].

We report here results for ozone photodissociation in the Hartley band. The photodissociation proceeds primarily via two spin-allowed channels, $O(^1D_2) + O_2(a\,^1D_g)$ and $O(^3P_J)+O_2(X\,^3\Sigma_g^-)$, with dominant ($\sim 90\%$) singlet products [3–5]. It has been known that the initial transition takes place exclusively to the $^1B_2$ (B) surface and about 10% yield of triplet products results from nonadiabatic crossing to the nearby R-state [6].

For measuring the alignment effects, we used linearly polarized photolysis and probe light to probe O($^1D_2$) using 2+1 REMPI scheme via $^1F_3$ state [7]. The fitting results of the difference image with appropriate basis functions indicates that the alignment effect due to an incoherent parallel excitation is significant for all coincident vibrational levels, which is consistent with previous measurements by Houston and coworkers [8]. As mentioned previously, since the angular momentum polarization is sensitive to the REMPI probe scheme, a different apparent angular distribution is obtained using a different probe scheme (2+1 REMPI via $^1P_1$ state) that has a much higher sensitivity to rank 4 moments. In this instance, we should consider the higher order effects to analyze the results in more detail and work is currently underway in our group.

Using circularly polarized probe light, the orientation in O($^1D_2$) at 266nm photodissociation have been measured [9]. The dissociation laser was polarized either circularly or linearly at 45° with respect to the time-of-flight axis in order to investigate the three possible atomic orientation parameters: that resulting from the incoherent perpendicular excitation (α_1) and the coherent excitation of parallel and perpendicular transition(γ_1, γ_1'). The results show that α_1 and γ_1 probed by circularly polarized photolysis light are negligible within the statistical error. In the other hand, γ_1' obtained by 45° linearly polarized light is significant and also strongly recoil-dependent. A fascinating aspect of the results is the change in sign of the innermost ring. To investigate the recoil-speed dependence of γ_1' more closely, we carried out a measurement of orientation effect at several photolysis wavelengths. The abrupt change of orientation effect is shown around 1300 m/s, that is, the value of γ_1' is small and positive for the slower fragments while large and negative for the faster fragments.

As already mentioned, the initial transition exclusively happens to the B state, whose transition dipole moment has both parallel and perpendicular components with respect to the light polarization vector. This provides a means to generate a coherent contribution even though the excitation is to a single surface, ultimately allowing for a large γ_1' orientation effect. However, this "static" coherence by itself cannot be a sufficient explanation for the profound speed dependence. Recently, Baloïtcha and Balint-Kurti calculated accurate potential energy surfaces of ozone with several avoided crossings [10]. There are two major curve crossings (B-A, B-R) related to dissociation processes yielding asymptotic singlet products. Based on their diabatic and adiabatic potential energy surfaces, we computed the probabilities of these two pathways using the Landau-Zener formula. One pathway is the diabatic dissociation along the B state and the other is the adiabatic dissociation crossing to A and R states. The results show a substantial speed-dependence to the overall crossing probability consistent with the following interpretation: For the fast fragments, the diabatic pathway is dominant showing a large negative orientation, while both adiabatic and diabatic pathways yield important contributions to the dissociation dynamics simultaneously for the slower fragments. It is likely that smaller modulations are superimposed

on these larger effects and associated with additional pathways and long-range nonadiabatic interactions.

---

[1] E. R. Wouters, M. Ahmed, D. S. Peterka, A. S. Bracker, A. G. Suits and O. S. Vasyutinskii, in *"Imaging in Chemical Dynamics"*, ed. by A. G. Suits and R. E. Continetti (American Chemical Society, Washington DC, 2000), p.238.

[2] D. Townsend, M. P. Minitti and A. G. Suits, Rev. Sci. Instr. **74**, 2530 (2003).

[3] C. E. Fairchild, E. J. Stone and G. M. Lawrence, J. Chem. Phys. **69**, 3632 (1978).

[4] R. K. Sparks, L. R. Carlson, K. Shobatake, M. L. Kowalczyk and Y. T. Lee, J. Chem. Phys. **72**, 1401 (1980).

[5] J. J. Valentini, D. P. Gerrity, J.-C. N. Phillips and K. D. Tabor, J. Chem. Phys. **86** , 6745 (1987).

[6] Z.-W. Qu, H. Zhu and R. Schinke, Chem. Phys. Lett. **377**, 359 (2003).

[7] D. Townsend, W. Li, S. K. Lee, R. L. Gross and A. G. Suits, J. Phys. Chem. A (2005), in press.

[8] S. M. Dylewski, J. D. Geiser and P. L. Houston, J. Chem. Phys. **115**, 7460 (2001).

[9] S. K. Lee, D. Townsend, O. S. Vasyutinskii and A. G. Suits, J. Phys. Chem. A (2005), in press.

[10] E. Baloïtcha and G. G. Balint-Kurti, J. Chem. Phys. **123**, 014306 (2005).

G. G. Balint-Kurti and M. P. de Miranda (eds.)
Vector Correlation and Alignment in Chemistry

Experimental technique for measurement of velocity dependent alignment and orientation of product molecules

David W. Chandler,[1] Elisabeth Wade,[1] K. Thomas Lorenz,[1] James W. Barr,[2] Wenwu Chen,[2] George L. Barnes,[2] and Joseph I. Cline[2]

[1] *Combustion Research Facility, P.O. Box 969, MS9055, Sandia National Laboratory, Livermore, CA USA 94550*
[2] *Department of Chemistry and Chemical Physics Program, University of Nevada, Reno, NV USA 89557*

I. INTRODUCTION

Crossed molecular beam experiments provide a wealth of detailed information on inelastic and reactive bimolecular collisions [1]. Scalar quantities measured in such experiments include chemical reaction probabilities and energy partitioning among the various product states. Measurements of vector quantities reveal the spatial angular correlations among the directional properties of the reactant and product trajectories. The vector quantity measured in traditional crossed beam experiments is the differential cross section (DCS), which gives the probability of product formation as a function of the angle θ between the initial relative velocity vector of the approaching reactants, $\mathbf{v}$, and the product ejection velocity vector, $\mathbf{v}'$. Product state distributions and DCS measurements provide essential data that discriminate among proposed mechanisms for chemical reactions.

Recently, several theoretical studies have calculated additional vector properties which are highly sensitive to the reaction mechanism and topology of the potential energy surface (PES) along the reaction pathway [2]. Of extreme importance is the center-of-mass frame $\mathbf{v}$-$\mathbf{v}'$-$\mathbf{j}'$ angular correlation among the directions of reactant approach $\mathbf{v}$, product ejection $\mathbf{v}'$, and product angular momentum, $\mathbf{j}'$. Recent advances in Doppler spectroscopy [3], TOF techniques [4], and ion imaging measurements [5] allow experimental measurement of the full $\mathbf{v}$-$\mathbf{v}'$-$\mathbf{j}'$ correlation, which includes both the $\mathbf{j}'$ *alignment* (the preferred *plane* of product rotation) and the $\mathbf{j}'$ *orientation* (the preferred *sense* of product rotation) with respect to the *scattering plane* defined by $\mathbf{v}$ and $\mathbf{v}'$. Recent studies of product rotational *alignment* in bimolecular collisions have probed reaction collisions with linearly polarized Doppler spectroscopy [6] and rotationally inelastic collisions with polarized REMPI spectroscopy [7]. We have recently published the details [8, 9] of our studies on the alignment and orientation of NO following

a collision with an Ar atom and here give an overview of those experiments.

Experimental techniques now exist for the determination of the aligment and orientation of product molecules and atoms as a function of angle and speed produced from either a unimolecular or a bimolecular interaction. Our experiments study rotationally inelastic collisions of nonrotating, nonvibrating, ground electronic state NO molecules with Ar atoms,

$$\mathrm{NO}\,^2\Pi_{1/2}(v=0, j=1/2) + \mathrm{Ar} \rightarrow \mathrm{NO}\,^2\Pi_{1/2}(v'=0, j') + \mathrm{Ar},$$

at a center-of-mass (CM) frame collision energy of 65 meV ($520 \pm 70\,\mathrm{cm}^{-1}$). The highest NO rotational state that can be populated at this collision energy is $j' = 16.5$. Note that the nonrotating NO molecule has $j = 1/2$ arising from the spin of its unpaired electron, which we will ignore in the following simple discussion. In a collision with Ar the initial NO trajectory $\mathbf{v}$ is deflected through the angle θ, resulting in a final NO product velocity $\mathbf{v}'$ and angular momentum $\mathbf{j}'$. In general the $\mathbf{j}'$ vector also has an in-plane component when the NO internuclear axis is initially out of the scattering plane, or if there are out-of-plane forces. The experiment samples a statistical distribution of initial NO impact parameters b and tilt angles, α, of the molecule with respect to the incoming atom.

II. EXPERIMENTAL APPARATUS

Our experimental technique combines a standard crossed molecular beam apparatus with laser photoionization and subsequent imaging of the scattered products. The molecular beams cross at a right angle and are 0.8 mm in diameter at the crossing point where scattering occurs. They are formed by skimming and collimating supersonic expansions, one of neat Ar and the other of 4% NO seeded in Ar produced by pulsed piezoelectric valves. Scattered NO molecules are state selectively ionized using $1{+}1'$ resonant enhanced multiphoton ionization through the R_{21} branch of the $A\,^2\Sigma^+_{1/2} \leftarrow X\,^2\Pi_{1/2}$ transition. This is accomplished with two laser pulses passing through the scattering region 10 ns apart. The first, "probe" laser pulse at ∼225 nm is either linearly polarized and in the plane of the molecular beams or circularly polarized and perpendicular to the plane containing the two molecular beams with its wavelength precisely tuned to excite a single NO rotational level, j', to the A electronic state. The second, "ionization" laser pulse at 302 nm ionizes NO A state molecules. Velocity-mapping ion optics accelerate the NO^+ onto a two-dimensional position sensitive microchannel plate detector coupled to a phosphor screen viewed by a cooled CCD camera.

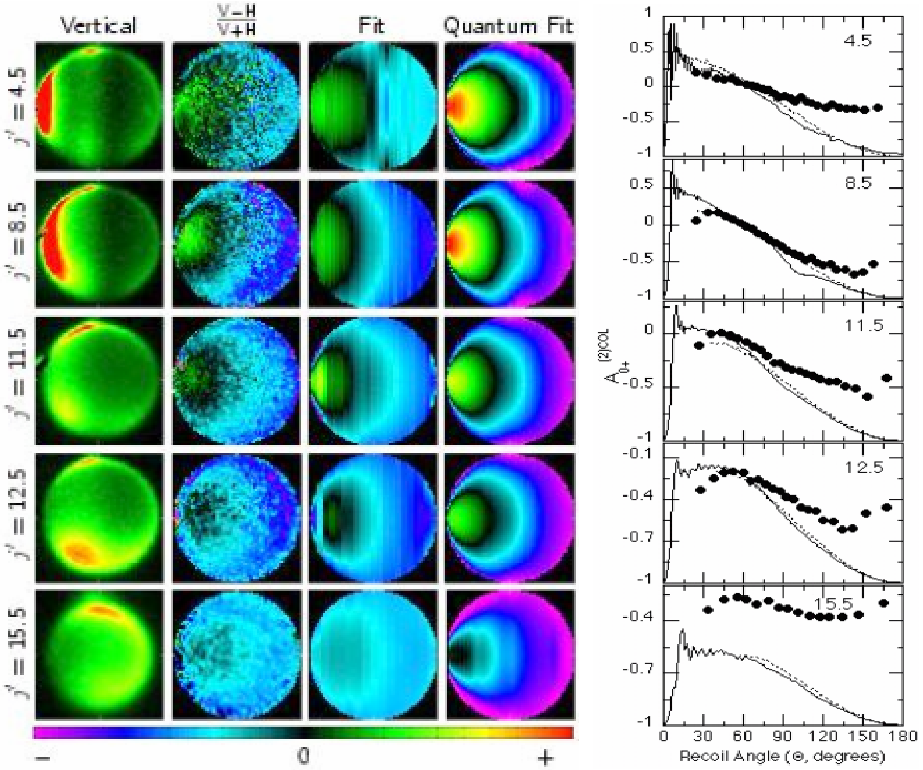

FIG. 1: Left: images taken with vertically polarized light, difference images ((V − H)/(V + H)), fitted difference images and difference images generated from calculation of alignment (see text). Right: Alignment moments, $A_{0+}^{(2)\mathrm{PRB}}(j', \Theta, \chi, \chi_p)$, extracted from images along with calculated alignment moments.

III. RESULTS

The captured ion image represents a two-dimensional projection of the product recoil velocity distribution onto the detector plane. We detect the NO product alignment by comparing its photoionization probability, as indicated by the intensity of the image at any given position, for horizontal and perpendicular linearly polarized probe light. The ion images for V polarization for each rotational state are shown in the first column of Figure 1. The second column shows normalized difference images, constructed by computing $(I_\mathrm{V} - I_\mathrm{H})/(I_\mathrm{V} + I_\mathrm{H})$ from the intensities I_V and I_H at each pixel location in the V and H images.

The third column shows the least squares fit of the normalized difference images used to extract alignment moments, as discussed in reference 9. The fourth column shows the theoretical predictions of the normalized difference images.

The experimental (V−H)/(V+H) images in Figure 1 reveal some trends. In all of the $(\mathrm{V}-\mathrm{H})/(\mathrm{V}+\mathrm{H})$ images, $I_\mathrm{H} > I_\mathrm{V}$ dominates overall but is concentrated in the back-scattered regions. For the lowest j states, $j' = 4.5$ and 8.5, the most forward-scattered products show some $I_\mathrm{V} > I_\mathrm{H}$ character. The extent of the forward-scattered $I_\mathrm{V} > I_\mathrm{H}$ pattern diminishes with increasing j', and in the $j' = 11.5$ image, the most forward-scattered products show $I_\mathrm{V} \sim I_\mathrm{H}$. For $j' = 15.5$, the $I_\mathrm{V} \sim I_\mathrm{H}$ pattern has further diminished so that nearly the entire image shows $I_\mathrm{H} > I_\mathrm{V}$ character.

These intensity patterns can be interpreted qualitatively by a simple model. The NO($A\,^2\Sigma \leftarrow X\,^2\Pi$) probe transition is polarized perpendicular to the molecular axis. The selection rules for the R_{21}-branch transitions require the j-vector to be perpendicular to both the transition dipole and the molecular axis. Since the absorption cross section is largest when the laser polarization is aligned with the transition dipole, $I_\mathrm{H} > I_\mathrm{V}$ character indicates that the NO internuclear axis lies preferentially in the scattering plane and when $I_\mathrm{V} > I_\mathrm{H}$ behavior dominates, the NO internuclear axis is preferentially perpendicular to the scattering plane.

$A_{0+}^{(2)\mathrm{PRB}}(j', \Theta, \chi, \chi_p)$ and $A_{2+}^{(2)\mathrm{PRB}}(j', \Theta, \chi, \chi_p)$ are the two leading alignment moments of a spherical tensor expansion of the angular distribution of $\mathbf{j}'_\mathrm{NO}$, which we will generally refer to as differential alignment moments. The value of $A_{0+}^{(2)\mathrm{COL}}(j', \Theta)$, shown in Figure 1, gives the propensity of the $\mathbf{j}'$-vector to point along $\mathbf{v}_\mathrm{NO}$. When $A_{0+}^{(2)\mathrm{COL}}(j', \Theta) = 2$, the $\mathbf{j}'$-vector is parallel to $\mathbf{v}_\mathrm{NO}$ (which is Z in the collision frame). When $A_{0+}^{(2)\mathrm{COL}}(j', \Theta) = -1$, the $\mathbf{j}'$-vector is perpendicular to $\mathbf{v}_\mathrm{NO}$.

We detect the NO product sense of rotation in the detector plane by comparing its photoionization probability for right (RCP) and left (LCP) circularly polarized probe light. For instance, when the NO is probed *via* R_{21} branch transitions, RCP probe light preferentially ionizes molecules with a CCW sense of rotation, as viewed by an observer looking towards the source of the probe light. Molecules with a CW sense of rotation are preferentially ionized by LCP light. Using the Hertel-Stoll [10] description of angular momentum polarization, the $Q(\theta)$ ratio can be shown to be

$$Q(\theta) = \frac{3h^{(1)}A_{1-}^{1}(\theta)}{2 + h^{(2)}\left[A_{0+}^{2}(\theta) + 3A_{2+}^{2}(\theta)\right]/2},$$

where the $A_{q+}^{k}(\theta)$ are deflection angle dependent real moments of the angular distribution of $\mathbf{j}'$, and $h^{(1)}$ and $h^{(2)}$ are specific to the branch and rotational level of the probe transition.

The mathematical sign of $Q(\theta)$, and the preferred sense of NO product rotation, is determined only by A_{1-}^{1}. We have calculated the $A_{q+}^{k}(\theta)$ moments

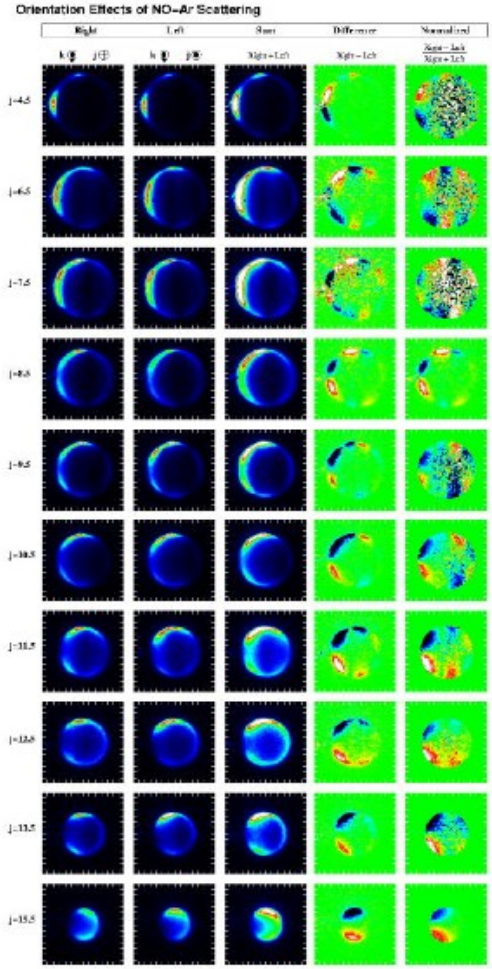

FIG. 2: Images obtained using right circularly polarized light, left circularly polarized light, the sum of those two images, the difference of those two images and the normalized difference image for several rotational states.

directly from the scattering matrix obtained in full close-coupled quantum calculations using two recent *ab initio* NO-Ar potentials of Alexander and the Hybridon scattering package [11]. The agreement is quite good for all quantum states measured.

IV. CONCLUSION

We have combined a new technique - crossed molecular beam ion imaging, with a new laser geometry and data analysis to extract alignment and orintation moments from images that are sensitive to the product alignment and orientation as a function of rotational state and scattering angle. The observation of a high degree of preference for molecular alignment and rotation created by simple inelastic scattering and the sensitivity of the orientation to details of the intermolecular potential make this an ideal case for testing *ab initio* potential energy surfaces. This should be true for reactive scattering as well because very specific reactive trajectories prevail and there are stringent requirements for reactant orientation. The alignment and orientation moments are extracted and compared with calculations using Alexander's CCSD(T) PES's. The theoretical and experimental alignment moments show excellent agreement for low Δj. For high Δj collisions and back-scattered trajectories, which sample the hard wall of the PES, the theoretical and experimental alignment moments show less agreement. The observed sense of NO product rotation (clockwise or counterclockwise) varies with deflection angle and is a strong function of the NO final rotational state. The largest preferences for sense of rotation are observed at the highest kinematically allowed product rotational states; for lower rotational states the variation with deflection angle becomes oscillatory. The quantum calculations show that measurements of the preferred sense of rotation are very sensitive to the intermolecular potential. Quantum calculations on the most recently reported NO-Ar potential give good agreement with the observed oscillation patterns in sense of rotation with deflection angle.

---

[1] See for example: P. Casavecchia, Rep. Prog. Phys. **63**, 355 (2000) and D. A. Case and D. R. Herschbach, J. Chem. Phys. **64**, 4212 (1976).

[2] See for example: F. J. Aoiz, M. Brouard, P. A. Enriquez, J. Chem. Phys. **105**, 4964 (1996) and M. P. de Miranda and D. C. Clary, J. Chem. Phys. **106**, 4509 (1997).

[3] See for example: J. P. Simons, Faraday Discuss. **113**, 1 (1999) and R. N. Zare, Science **279**, 1875 (1998).

[4] See for example: S. A. Kandel, A. J. Alexander, A. J. Kim, R. N. Zare, F. J. Aoiz, L. Bañares, J. F. Castillo and V. S. Rabanos, J. Chem. Phys. **112**, 670 (2000) and H. Meyer, J. Chem. Phys. **102**, 3151 (1995).

[5] See for example: T. P. Rakitzis, P. C. Samartis and T. N. Kitsopoulos, J. Chem. Phys. **111**, 10415 (1999) and A. G. Suits, L. S. Bontuyan, P. L. Houston and B. J. Whitaker, J. Chem. Phys. **96**, 8618 (1992).

[6] See for example: H. Meyer, J. Phys. Chem. **101**, 6697 (1994).

[7] J. I. Cline, K. T. Lorenz, E. A. Wade, J. W. Barr and D. W. Chandler, J. Chem. Phys. **115**, 6277 (2001).

[8] K. T. Lorenz, D. W. Chandler, J. W. Barr, W. Chen, G. L. Barnes and J. I. Cline, Science **293**, 2063 (2001).
[9] E. A. Wade, K. T. Lorenz, D. W. Chandler, J. W. Barnes and J. I. Cline, Chem. Phys. **301**, 261 (2004).
[10] I. V. Hertel and W. Stoll, Adv. At. Mol. Phys. **13**, 113 (1977).
[11] M. H. Alexander, J. Chem. Phys. **111**, 7426 (1999).

G. G. Balint-Kurti and M. P. de Miranda (eds.)
Vector Correlation and Alignment in Chemistry

Exact and model descriptions of the stereodynamics of bimolecular collisions

Marcelo P. de Miranda
School of Chemistry, University of Leeds, Leeds LS2 9JT, United Kingdom

I. INTRODUCTION

Articles on the stereodynamics of molecular collision and fragmentation processes almost invariably cite the need for deeper understanding of the mechanisms of such processes as the main motivation for their study. The idea is that analysis of the very detailed information contained in vector properties will lead to a matching level of detail in the understanding of the dynamics.

As an inspection of this booklet will show, groups around the world have developed a variety of methods for the measurement and calculation of vector properties. (We have contributed to that effort ourselves — see, for instance, Refs. 1–5). We believe, however, that the data accumulated so far has not yet fulfilled their promise. While progress has been achieved, understanding of molecular collision and fragmentation dynamics has not yet advanced to the point of allowing one to unambiguously explain the whys and hows of detailed, state-to-state, angle-resolved vector properties.

Our recent work has included attempts at methods allowing for increased insight rather than increased level of detail. This article briefly considers two of those: the time-dependent description of the stereodynamics of bimolecular collisions, and a simple geometrical model for the stereodynamics of such processes. The other techniques we have recently developed have been discussed elsewhere (see the article by F. J. Aoiz in this booklet and also Refs. 5–9).

II. TIME-DEPENDENT STEREODYNAMICS

In his recent work, Althorpe has shown how scattering matrices obtained in energy-domain calculations can be transformed into their time-domain counterparts and vice-versa [10–12], possibly with the use of "filters" allowing for the decomposition of the scattering amplitude (and, therefore, also the differential cross section and other vector properties) into contributions from scattering mechanisms that can be separated in either domain.

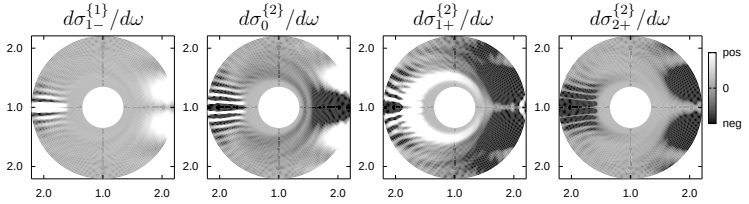

FIG. 1: Energy-domain unnormalised PDDCSs of reaction (1). Radius gives collision energy in eV ($E_{\rm coll} = 1\,$eV at the centre), scattering angle is $\theta = 0$ to the left and $\theta = 180^\circ$ to the right.

The transformations introduced in Althorpe's work make the calculation of time-domain vector properties straightforward: time-domain scattering matrices can be used in the previously published, energy-domain stereodynamical methods [1, 2] in exactly the same manner as their energy-domain counterparts.

Using scattering matrices obtained by the Althorpe group for the

$$\mathrm{H} + \mathrm{D}_2(v = 0, j = 0) \rightarrow \mathrm{HD}(v' = 3, j' = 1) + \mathrm{D} \qquad (1)$$

reaction, we have calculated the E- and t-domain unnormalised polarisation-dependent differential cross sections [4] shown on Figs. 1 and 2. (The units used for the PDDCSs are arbitrary, and were chosen in order to magnify the contrast between positive and negative values. The frame of reference is such that the z axis coincides with the product-recoil direction $\mathbf{k}'$ and the y axis coincides with $\mathbf{k} \times \mathbf{k}'$, where $\mathbf{k}$ is the reactant-approach direction.)

On one hand, comparison between Figs. 1 and 2 shows that vector properties can help the separation of reaction mechanisms and the establishment of correlation between results obtained in the time or energy domains. The time-domain separation of the "direct" and "time-delayed" mechanisms was first accomplished by Althorpe *et al.* in their study of reaction (1) when leading to the

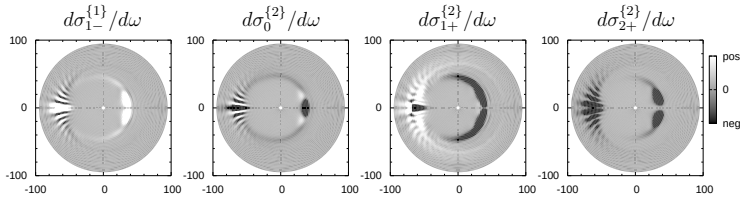

FIG. 2: Time-domain unnormalised PDDCSs of reaction (1). Radius gives time in fs, scattering angle is $\theta = 0$ to the left and $\theta = 180^\circ$ to the right.

HD($v' = 3, j' = 0$) product [13]. In that case, as in the one reported here, the DCS suffices for the separation. In the case of higher rotational states, however, consideration of the DCS only will not suffice [14].

On the other hand, detailed consideration of the vector properties displayed in Figs. 1 and 2 shows that, whatever the domain considered, identification of a detailed reaction mechanism is not easy [14]. This illustrates the comments made above: the more detailed results do not necessarily lead to a more detailed understanding.

III. GEOMETRICAL MODEL OF REACTION STEREODYNAMICS

In order to assist the interpretation of stereodynamical data, we have developed a simple, purely geometrical model of the stereodynamics of A + BC reactions. According to this model, which describes the dynamics in classical terms and with emphasis on its time-dependence, there are only two sources of product rotation: the (internal) torque caused by the break-up of the ABC intermediate complex, and the (external) torque caused by the overall rotation of the system [15].

In particular, we had hoped that this model might help explain the positive and negative values of the $d_{1+}^{\{2\}}/d\omega$ PDDCS, which quantifies product rotational alignment along the $x \pm z$ directions — in other words, preference for tilting of propeller-type rotational motion of the products towards or away from the reactant-approach direction. As propeller-type rotation of the bimolecular fragment requires an external torque (internal forces alone cannot lead to propeller-type rotation), we in particular expected the results to allow for a rationalisation of the role of overall rotation in the collision stereodynamics.

As might be expected for such a simple model, the results obtained were mixed [14]. While allowing for a qualitative explanation of some general aspects of the stereodynamics, the model results did not lead to unambiguous interpretation of the exact data. In our opinion, this points toward a need for better models, a topic to which we plan to devote future work.

Acknowledgements. The work reviewed here resulted from collaborative work, and it is with great pleasure that the author acknowledges the invaluable contributions by S. C. Althorpe, R. A. Pettipher and J. M. Haigh. Financial support from EPSRC and the University of Leeds is also gratefully acknowledged.

---

[1] M. P. de Miranda and D. C. Clary, J. Chem. Phys. **106**, 4509 (1997).
[2] M. P. de Miranda, S. K. Pogrebnya and D. C. Clary, Faraday Discuss. **113**, 119 (1999).

[3] M. P. de Miranda, S. Crocchianti and A. Laganà, J. Phys. Chem. A **103**, 10776 (1999).
[4] M. P. de Miranda, F. J. Aoiz, L. Bañares and V. Sáez-Rábanos, J. Chem. Phys. **111**, 5368 (1999).
[5] J. Aldegunde, M. P. de Miranda, J. M. Haigh, B. K. Kendrick, V. Sáez-Rábanos and F. J. Aoiz, J. Phys. Chem. A **109**, 6200 (2005).
[6] F. J. Aoiz, J. Aldegunde, V. Sáez-Rábanos, B. K. Kendrick and M. P. de Miranda, submitted to Phys. Rev. Lett.
[7] M. P. de Miranda, in *Semiclassical and Other Methods for Understanding Molecular Collisions and Chemical Reactions*, ed. by D. Sokolovski, J. N. L. Connor and S. Sen (CCP6, Warrington, in press).
[8] M. P. de Miranda and F. J. Aoiz, Phys. Rev. Lett. **93**, 083201 (2004).
[9] M. P. de Miranda, F. J. Aoiz, V. Sáez-Rábanos and M. Brouard, J. Chem. Phys. **121**, 9830 (2004).
[10] S. C. Althorpe, Int. Rev. Phys. Chem. **23**, 219 (2004).
[11] S. C. Althorpe, J. Chem. Phys. **121**, 1175 (2004).
[12] S. C. Althorpe, Phys. Rev. A **69**, 042702 (2004).
[13] S. C. Althorpe, F. Fernandez-Alonso, B. D. Bean, J. D. Ayers, A. E. Pomerantz, R. N. Zare and E. Wrede, Nature **416**, 67 (2002).
[14] R. A. Pettipher, M. P. de Miranda and S. C. Althorpe, to be published.
[15] R. A. Pettipher, J. M. Haigh and M. P. de Miranda, to be published.

G. G. Balint-Kurti and M. P. de Miranda (eds.)
Vector Correlation and Alignment in Chemistry

The state-to-state-to-state model of direct chemical reactions*

Rex T. Skodje[1,2]

[1]*Institute of Atomic and Molecular Sciences, Academia Sinica, PO Box 23-166, Taipei, Taiwan*
[2]*Department of Chemistry and Biochemistry, University of Colorado, Boulder, CO 80309, USA*

The idea of the transition state has proven to be one of the most useful concepts employed by chemists to understand the behavior of chemical reactions [1]. The initial motivation for the transition state idealization was to provide a method (transition state theory, TST) to compute reaction rate constants from the local dynamics near the barrier without the need to follow the full collision dynamics. However, it is widely appreciated that the properties of the transition state can also be used to rationalize or predict the properties of the detailed reaction dynamics. A famous example is the "Polanyi rule" that, *e.g.*, correlates the location of the saddlepoint to the role of vibrational excitation in promoting the reaction rate. A variety of studies have qualitatively (or semi-quantitatively) explored the connection between the transition state and the final ro-vibrational state distribution, as well some gross aspects of the angular product distribution [2–6]. What has been missing until now is a quantitative theory that provides a means to compute the state resolved differential cross section (DCS) directly from the transition state. Here, we outline our approach, called the "state-to-state-to-state" theory of reactions that gives such a method [7–10]. When accurate, this theory provides a basis to understand the angular and state specific product distribution of a reaction as quantities set by the passage through the transition state. Obviously, we expect that such an approach is reasonable only when the initial and final channel interactions are small enough so that the reagent (product) are not significantly altered by the potential before (or after) the transition state. Therefore, highly polar species and systems with deep van der Waals wells are eschewed and we shall only discuss direct chemical reactions.

---

* This work has been done in collaboration with Magnus Gustafsson and the experimental group of Xueming Yang.

A major advance in the analysis of the quantum dynamics near the TS was the introduction of the notion of the quantum bottleneck state (QBS). The QBS are unstable quantum states perched at the top of dynamical barriers and can be assigned to the internal ro-vibrational states of the collision complex [11, 12]. Unlike conventional resonance states, QBS correspond to a sequence of poles in the complex energy space, with complex energies (in the parabolic limit) given by $z_n = V_0 - i\hbar\omega(n + 1/2)$ where ω is the barrier frequency and V_0 is the barrier height. The $n = 0$ (dominant) pole and the associated Seigert-state wavefunction can be used for many aspects of the physical analysis but the full pole spectrum is naturally required to correctly model the barrier transmission. We have introduced the "spectral quantization method" as a means to compute the QBS wavefunction and complex energy (for the dominant pole) [13]. The key theoretical distinction between the QBS and the simple TST formulation is that the QBS can be found exactly from full quantum mechanics (near the barrier) and ambiguities about coordinate system and internal mode coupling thus avoided. Truhlar and coworkers in particular have made major advances in the use the QBS to analyze the control of reactivity observed in exact quantum scattering simulations (at constant total angular momentum, J).

While the QBS provide a very useful and rigorous means to quantify the quantum state structure of the TS, they have proven be notoriously difficult to observe directly in the laboratory Working in collaboration with Yang, these signatures were observed in elementary chemical reactions using a molecular beam apparatus that employs the highly sensitive Rydberg tagging method of product detection [14]. Not only were the experimental results predicted, but the resulting theory provides new insights into the outcome of chemical reactions. Briefly, there were two strategies invoked. In the first, the QBS were observed through a manifestation of the time-delay associated with passage across the dynamical barrier. In the second, an interference structure was predicted and observed associated the passage through multiple QBS pathways through the TS.

The underlying state-to-state-to-state model of chemical reactions is illustrated schematically in Fig. 1. The incoming reagent is imagined to be concentrated in a single ro-vibrational state. Due to coupling, this incident flux is distributed among the reagent states in the entrance channel. Near the transition state, the QBS states are assumed to provide a good basis (since they solve $H\Psi = z\Psi$) and the passage through the transition state region is assume to be separable. That reactive steps are observed in the exact QM $N_R(E, J)$ is evidence to this fact. Then, the coupling acts again in the exit channel to scramble the outgoing flux among the product ro-vibrational states. The picture that emerges of the detailed dynamics is that of interfering pathways through the TS. That is, a given state-to-state reaction probability is coherent superposition of amplitudes passing the TS through different QBS paths. This physical picture

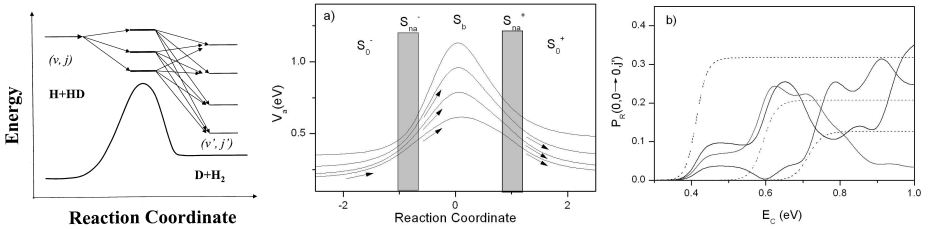

FIG. 1: A schematic diagram of the state-to-state-to-state picture of chemical reactions. The incident reactive flux passes the transition state a number of accessible QBS. The nonadiabatic couplings are assumed to occur in the channels, so that the passage through the TS is separable in the QBS basis.

can be expressed mathematically by writing the S-matrix as

$$\mathbf{S}(E) = \mathbf{S}_0^- \cdot \mathbf{S}_{na}^- \cdot \mathbf{S}_b \cdot \mathbf{S}_{na}^+ \cdot \mathbf{S}_0^+. \tag{1}$$

Here the $\mathbf{S}_b$ term models the barrier crossing dynamics and is assumed to be diagonal in the QBS representation and can be written in terms of one-dimensional barrier crossing amplitudes. The terms, $\mathbf{S}_{na}^{\pm}$, induce transitions between the rovibrational states of the products (reactants) and are matched to the QBS states. The terms $\mathbf{S}_0^{\pm}$ represent free asymptotic motion and can be used to accomplish frame transformations. This decomposition of the S-matrix is attractive since its reactive trace yields the VTST result for $N_R(E, J)$. This expression can be used to fully express the DCS in a manner that brings out the influence of the transition state very directly. It is found that the interference of coherent pathways through the TS lead to generic oscillations in the detailed state to state observables. Thus, the smooth oscillations that are routinely observed in state resolved reactive DCS's are often nothing more than the natural behavior of the passage through a multidimensional TS. Furthermore, the influence of reagent orientation (or product polarization) is naturally understood in terms of the symmetry of the QBS. As an added bonus, it appears that certain aspects of stereo-dynamics can be inferred from the results of (unoriented) conventional molecular beam experiments using an analysis based on the state-to-state-to-state model.

---

[1] D. G. Truhlar, B. C. Garrett and S. J. Klippenstein, "Current Status of Transition-State Theory," J. Phys. Chem. **100**, 12771 (1996).

[2] R. Schinke, R. L. Vander Wal, J. L. Scott and F. F. Crim, J. Chem. Phys. **94**, 283 (1991).

[3] I. R. Elsum and R. G. Gordon, J. Chem. Phys. **76**, 3009 (1982).
[4] G. C. Schatz and J. Ross, J. Chem. Phys. **66**, 1037 (1976).
[5] D. C. Clary, J. Chem. Phys. **96**, 3656 (1991).
[6] D. Wang and J. M. Bowman, Chem. Phys. Lett. **207**, 227 (1993).
[7] S. A. Harich, D. Dai, C. C. Wang, X. Yang, S. D. Chao and R. T. Skodje, Nature **419**, 281 (2002).
[8] D. Dai, C. C. Wang, S. A. Harich, X. Yang, S. D. Chao and R. T. Skodje, Science **300**, 1730 (2003).
[9] R. T. Skodje and X. Yang, Int. Rev. Phys. Chem. **23**, 253 (2004).
[10] S. D. Chao, S. A. Harich, D. X. Dai, C. C. Wang, X. Yang and R. T. Skodje, J. Chem. Phys. **117**, 8341 (2002).
[11] D. C. Chatfield, R. S. Friedman, D. C. Schwenke and D. G. Truhlar, J. Phys. Chem. **96**, 2414 (1992).
[12] T. Seideman and W. H. Miller, J. Chem. Phys. **95**, 1768 (1991).
[13] R. Sadeghi and R. T. Skodje, J. Chem. Phys. **102**, 193 (1995).
[14] L. Schneider et al, Science **269**, 207 (1995).

G. G. Balint-Kurti and M. P. de Miranda (eds.)
Vector Correlation and Alignment in Chemistry

Effect of the reactants polarization on the $H + D_2(v = 0, j = 2)$ reaction cross section near the threshold

F. Javier Aoiz,[1] Marcelo P. de Miranda,[2]
V. Sáez-Rábanos,[3] and Jesús Aldegunde[4]

[1]*Departamento de Química Física, Facultad de Química, Universidad Complutense, 28040 Madrid, Spain*
[2]*School of Chemistry, University of Leeds, Leeds LS2 9JT, United Kingdom*
[3]*Departamento de Química y Bioquímica, Escuela Técnica Superior de Ingenieros de Montes, Universidad Politécnica de Madrid, 28040 Madrid, Spain*
[4]*Departamento de Química Física, Facultad de Ciencias Químicas, Universidad de Salamanca, Salamanca, Spain*

I. INTRODUCTION

That the polarization of the rotational angular momenta and hence of the molecular axes of the reactants play a key role on the reactivity is part of the common wisdom in Reaction Dynamics. The detailed knowledge of the role of directional effects on the scattering observables has a crucial importance in understanding the reaction mechanism and the forces that are inherent to a chemical reaction. In addition, there is an great interest in devising techniques allowing the control of molecular collisions, either to maximize or minimize the reactivity or to select desired collision outcomes.

A new methodology has been proposed by us [1] in order to calculate in a rigourous way the effect of the polarization of the reagent's rotational angular momentum on the reactivity. The theory is based on the dichotomy of "intrinsic" and "extrinsic" polarization moments. The former describe the reactive process itself and quantify the dependence of the reaction cross section on the anisotropies of the rotational angular momentum and molecular axis distributions of the reactants. Intrinsic polarization moments are inherently determined by the collision dynamics rather than by external circumstances. Extrinsic polarization moments account for actual reactant preparation schemes, and quantify the anisotropies of the rotational angular momentum and molecular axis distributions in the asymptotic region where reactants do not yet interact, and they are a consequence of external circumstances (the experimental setup) rather

than the reaction itself; they have nothing to do with the collision dynamics. Of course, the values of the reaction properties cannot be calculated unless the reactant state (extrinsic property) is well defined, but the dynamical information is in the intrinsic properties.

The methodology is illustrated with results obtained for the prototypical $H+D_2$ reaction at low collision energies not far from the reaction threshold. It is shown that under conditions experimentally achievable, by changing the direction of the light polarization vector used for stimulated Raman pumping, the alignment of the D_2 molecules has striking effects on the total reaction cross section and the product's rotational distribution.

II. THEORETICAL METHOD

The methodology and the underlying theory employed in this work has been described in a recent article [1] and we thus refer to it for a full account of method used in this work. Here it suffices to say that intrinsic polarization parameters (PP), $s_q^{(k)}$, and polarization dependent differential cross sections (PDDCS), $S_q^{(k)}(\theta)$, are calculated using the full converged scattering matrix. These moments are referred to the *scattering frame*, whose z axis is along the initial relative velocity, $\mathbf{k}$ and the xz plane contains both $\mathbf{k}$ and final ($\mathbf{k'}$) relative velocities With these moments it is possible to construct *stereodynamical portraits* as a function of the angles θ_j and ϕ_j which define the direction of $\mathbf{j}$ in the scattering frame, revealing the chemical shape of the molecules in reactive collisions with other atoms or molecules into a particular state and/or scattering angle. These portraits provide a visual and compact idea of the preferred directions of the rotational angular momentum and internuclear axis for the reaction to take place. Sterodynamical portraits have been discussed in some recent publications [1–3].

In addition, when confronting possible experimental situations we will need to also consider a XYZ "laboratory frame", whose origin coincides with the scattering frame but whose spatial orientation is fixed. In this frame the direction of $\mathbf{j}$ is defined by the angles Θ_j and Φ_j. We choose to represent the relationship between the two frames in terms of the rotation that takes xyz into XYZ, and represent the Euler angles that define this rotation by α, β and γ, such that β and α are the polar and azimuthal angles which describe the orientation of Z in the scattering frame.

If reactants are produced in the laboratory with *extrinsic* polarization moments $A_Q^{(k)}$ referred to the space-fixed frame XYZ, the values of the scattering-

frame extrinsic polarization moments $a_q^{(k)}$ are simply given by

$$a_q^{(k)} = \sum_{Q=-k}^{k} D_{qQ}^{k*}(\alpha, \beta, \gamma) A_Q^{(k)}, \tag{1}$$

where $D^k(\alpha, \beta, \gamma)$ is a Wigner rotation matrix.

Once we have the two ingredients, extrinsic and intrinsic polarization moments, we can undertake the determination of the reaction integral cross section (which must take into account an actual, extrinsic reactant preparation scheme as well as the intrinsic reactants PP). It can be shown [1] that the integral cross section can be written as

$$\sigma = \sigma_{\mathrm{iso}} \sum_{k}^{2j} (2k+1) s_0^{(k)} a_0^{(k)} \tag{2}$$

where σ_{iso} is the integral cross section of the reaction involving unpolarized reactants, and only the polarization parameters with q=0 appear in the expression of the integral cross section σ. If all $a_q^{(k)}$ are zero except for k=0, q=0, that is, if the selection of the initial directions of $\mathbf{j}$ is isotropic, Eq. (2) yields the usual *unpolarized* ICS.

III. RESULTS

We have investigated the role of D_2 alignment in the dynamics of the

$$\mathrm{H} + \mathrm{D}_2(v=0, j=2) \rightarrow \mathrm{HD}(v'=0, j') + \mathrm{D} \tag{3}$$

reaction at collision energies at $E_{\mathrm{coll}} = 0.501\,\mathrm{eV}$. The dynamical calculations have been carried out on the BKMP2 potential energy surface [4] using time-independent quantum reactive scattering [5].

We next consider a plausible experiment involving the extrinsic alignment of $\mathbf{j}$. In simple terms, such experiment consists in the following: to place the molecules in the D_2 beam in the $|v=0, j=2, m=0\rangle$ state, where the magnetic quantum number is determined with regard to a laboratory-fixed quantization axis Z whose direction can be chosen. The preparation of this state can be achieved by pure rotational Raman scattering pumping by selecting the right pump and Stokes frequencies for stimulated Raman scattering. This amounts to preparing $D_2(v=0, j=2)$ molecules whose interatomic axis is aligned parallel/antiparallel to Z and whose rotational angular momentum is aligned perpendicular to Z. By varying the direction of the laboratory axis Z, one varies its direction with respect to the scattering-frame vector $\mathbf{k}$ and, if the experiment involves angle-resolved product detection, also with regard to the scattering plane, containing

k and **k**′). Given that the laboratory axis Z is also the axis with regard to which the D_2 molecules are aligned, changing the direction of Z with regard to **k** and possibly **k**′ amounts to changing the D_2 alignment in the scattering frame.

For the proposed case of a pure $|\,2,0\rangle$ state, the axial and rotational D_2 polarizations are both completely described by three $A_Q^{(k)}$ molecular polarization moments referred to the XYZ laboratory frame: the only nonvanishing moments are those with $k = 0$, 2 or 4 and $Q = 0$, and they take the values

$$A_0^{(0)} = 1, \qquad A_0^{(2)} = -\sqrt{\frac{2}{7}}, \qquad A_0^{(4)} = +\sqrt{\frac{2}{7}}. \tag{4}$$

In order to obtain the extrinsic reactants polarization moments in the xyz scattering frame, one has to use Eq. (1). It leads to

$$a_q^{(k)} = D_{q0}^{k*}(\alpha,\beta,\gamma)A_0^{(k)} = C_{kq}(\beta,\alpha)A_0^{(k)}. \tag{5}$$

Note that, as the distributions we are considering have cylindrical symmetry around Z and therefore all nonvanishing $A_Q^{(k)}$ moments have $Q = 0$, the only Euler angles required are α and β, the azimuthal and polar angles that specify the direction of the laboratory axis Z in the scattering frame. Moreover, it is easy to show that since only intrinsic PP, $a_q^{(k)}$ with q=0 appear in Eq. (2), the integral cross section will only depend on the β angle (azimuthally symmetric), and it will be denoted by σ^β.

We have selected an example so that the can highlight what can be achieved in a possible experiment, and to what extent it is possible to control the outcome of the reaction by varying the polarization of the reagents. Specifically, we have considered the values for the polar angle $\beta = 0°$, 54.74° or 90° [$\beta = 54.74°$ is the so-called "magic angle" at which $P_2(\cos\beta) = 0$]. When analyzing the data presented below, it will be useful to remember that the D_2 interatomic axis **r** and rotational angular momentum **j** are respectively aligned along or perpendicular to the direction specified by β.

Fig. 1 shows QM data illustrating the effect of the polar angle β on the integral cross section σ^β into v'=0, summed over all product rotational states at $E_{\rm coll}$=0.501 eV. The black solid bar corresponds to the usual cross section(without D_2 polarization), while the others include the effect of D_2 alignment. The dependence of the reaction cross section on reactant alignment is clear: reactivity is enhanced by head-on, collinear collisions ($\beta = 0°$, **r** and **j** respectively parallel and perpendicular to **k**), diminished by side-on collisions ($\beta = 90°$, **r** and **j** respectively perpendicular and parallel to **k**), and largely unaffected by alignment along the magic angle. For head-on collisions, with the internuclear axis aligned along **k**, the reactivity is enhanced by a factor of 2.5. This is not an unexpected result for the reaction we are considering here (the H + D_2 reaction has long been known to be collinearly-constrained), but

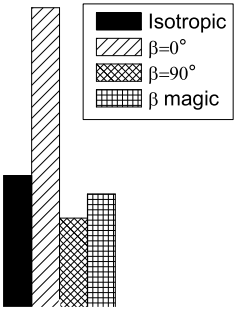

FIG. 1: Vibrationally resolved integral cross section for different alignment direction of the D_2 molecule. The β angle is the direction of the polarization vector of the pump laser with respect to the initial relative velocity.

it serves to quantify the extent to which the reactivity can be controlled by selective reactant polarization.

The effect of D_2 alignment on product rotational state distributions for HD formation into v'=0 at $E_{\rm coll} = 0.501\,{\rm eV}$ is clearly seen in Fig. 2, which shows the data obtained with the same β values considered above. Collinear collisions ($\beta = 0$) lead to a colder product rotational state distribution and considerable larger cross section for low j' values, while side-on collisions ($\beta = 90°$) result is a neat decrease of the cross section values. In particular, the cross section

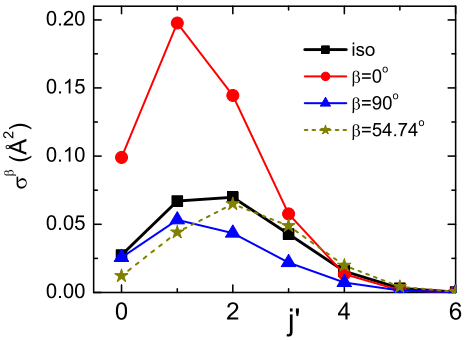

FIG. 2: HD rotational distribution from reaction (3) at $E_{\rm coll} = 0.501\,{\rm eV}$ as a function of the product rotational state for different D_2 alignment directions obtained by varying the β angle.

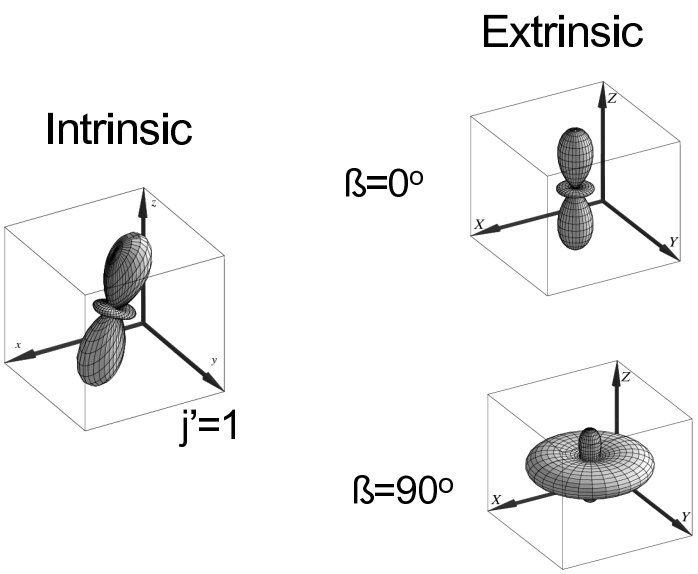

FIG. 3: Stereodynamical portraits showing the intrinsic (left panel) and extrinsic (top and bottom right panels) internuclear axis distributions. The intrinsic distribution corresponds to j'=1 produced in reaction 3 at $E_{\rm coll}$= 0.501 eV. The extrinsic distributions represents the internuclear axis distributions in the scattering frame when the molecule is aligned parallel (β=0°) or perpendicular (β=90°) with respect to the initial relative velocity vector.

leading to j'=1 is enhanced by a factor of three with respect to that with an isotropic distribution. Since there is cylindrical symmetry around the reactant-approach direction **k**, as shown by Eq. (2), the only polarization parameters that contribute to the integral cross section are $s_0^{\{0\}}$, $s_0^{\{2\}}$ and $s_0^{\{4\}}$; of these, $s_0^{\{2\}}$ is the one that is largely responsible for the polarization effects and the value of this parameter is close to its limiting negative value of -0.5 for j'=1. No surprise, then, that preparation of reactants with $a_0^{\{2\}} = -0.535$,(the quantum values of the extrinsic polarization moments corresponding to reactant alignment is along $\beta = 0$) lead to a considerable enhancement of the cross section for this particular state. This is more clearly seen in Fig. (3): the intrinsic distribution of internuclear axis matches very closely the extrinsic one for β=0°, whereas that for β=90° (with the internuclear axis mainly perpendicular to the relative velocity) clearly departs from the optimum distribution for j'=1 production.

The results so far considered show that D_2 polarization, and D_2 alignment in particular, can have a dramatic effect on the outcome of the H + D_2 collision.

By selecting specific directions for the D_2 alignment, we have obtained starkly contrasting reactive cross sections as well as starkly contrasting product state distributions.

---

[1] J. Aldegunde, M. P. de Miranda, J. M. Haigh, B. K. Kendrick, V. Sáez-Rábanos and F. J. Aoiz, J. Phys. Chem. A **109**, 6200 (2005).

[2] M. P. de Miranda and F. J. Aoiz, Phys. Rev. Lett. **93**, 083201 (2004).

[3] M. P. de Miranda, F. J. Aoiz, V. Sáez-Rábanos and M. Brouard, J. Chem. Phys. **121**, 9830 (2004).

[4] A. I. Boothroyd, W. J. Keogh, P. G. Martin and M. R. Peterson, J. Chem. Phys. **104**, 7139 (1996).

[5] B. K. Kendrick, J. Chem. Phys. **114**, 8796 (2001).

[6] S. A. Kandel, A. J. Alexander, Z. H. Kim, R, N. Zare, F. J. Aoiz, L. Bañares, J. F. Castillo and V. Sáez-Rábanos, J. Chem. Phys. **112**, 670 (2000).

G. G. Balint-Kurti and M. P. de Miranda (eds.)
Vector Correlation and Alignment in Chemistry

Time-dependent wave packet studies of hydrogen halide dissociation: polarization of atomic photofragments

Alex Brown
Department of Chemistry, University of Alberta, Edmonton, AB, T6G 2G2, Canada

I. INTRODUCTION

The hydrogen halides, HX (X = F, Cl, Br, and I), provide model systems for studying photodissociation dynamics on multiple potential energy curves (PECs) including non-adiabatic coupling effects. The photodissociation process

$$\begin{aligned} \mathrm{HX} + \mathrm{h}\nu &\rightarrow \mathrm{H}(^2\mathrm{S}) + \mathrm{X}(^2\mathrm{P}_{3/2}) \\ &\rightarrow \mathrm{H}(^2\mathrm{S}) + \mathrm{X}(^2\mathrm{P}_{1/2}) \end{aligned}$$

to yield ground and spin-orbit excited state halogen atoms has been of both experimental and theoretical interest, see, for example[1–12]. An understanding has been sought of the roles of the various electronic states involved in the excitation and the possible non-adiabatic transitions that could take place between the excited PECs as the molecule fragments. If spin-orbit coupling is included, there are twelve adiabatic electronic states correlating with the above product channels. The $\mathrm{X}^1\Sigma_{0+}$ (ground state), $\mathrm{A}^1\Pi_1$ (two substates), $\mathrm{a}^3\Pi_1$ (two substates), $\mathrm{a}^3\Pi_2$ (two substates), and $\mathrm{a}^3\Pi_{0-}$ states correlate with the $\mathrm{H}(^2\mathrm{S}) + \mathrm{X}(^2\mathrm{P}_{3/2})$ dissociation channel, while the $\mathrm{t}^3\Sigma_1$ (two substates), $\mathrm{a}^3\Pi_{0+}$, and $\mathrm{t}^3\Sigma_{0-}$ states correlate with $\mathrm{H}(^2\mathrm{S}) + \mathrm{X}(^2\mathrm{P}_{1/2})$ channel. While there are twelve adiabatic states, the states involved primarily in the dissociation are the optically accessible $\mathrm{A}^1\Pi_1$, $\mathrm{a}^3\Pi_1$, $\mathrm{t}^3\Sigma_1$, and $\mathrm{a}^3\Pi_{0+}$ states. The term symbols represent a mixed Hund's case(a)/case (c) according to ${}^{2S+1}L_\Omega$. When including the spin-orbit coupling, Ω is the only good quantum number and the ${}^{2S+1}L$ labels designate the largest case(a) contribution within the Franck-Condon region. The spin-orbit splittings between the two product channels are 404 cm^{-1}, 882 cm^{-1}, 3685 cm^{-1}, and 7603 cm^{-1}[13], for HF, HCl, HBr, and HI, respectively. Therefore, the effects of increasing spin-orbit coupling on the dissociation process can be examined systematically.

Most experimental and theoretical studies of the hydrogen halides have focused on determining the total cross-section, the branching fraction Γ, which

provides the yield of spin-orbit excited atoms ($X^2P_{1/2}$) relative to the total yield, and/or on the anisotropy parameter β, which provides information on the parallel and/or perpendicular nature of the electronic transitions contributing to the dissociation. While the measurement or computation of these properties has provided a wealth of information on the potential energy curves, transition dipole moments, and, if applicable, non-adiabatic couplings, underlying the dynamics, our recent work[14–18] has focused on calculating the $\mathbf{a}_Q^{(K)}(p)$ parameters describing the orientation and alignment of the halogen atoms in the molecular frame. Since the halogen atoms have angular momenta, they can have a preferred orientation and/or alignment in space and this can be fully described in the molecular frame by the $\mathbf{a}_Q^{(K)}(p)$ parameters[19]. K and Q refer to the spatial distributions in the molecular frame. The symmetry of the transition dipole moments from the ground electronic state to the dissociating states is given by p and can be $\parallel$, $\perp$, or $(\parallel, \perp)$ corresponding to pure parallel, pure perpendicular, or mixed parallel/perpendicular excitation. An equivalent set of anisotropy parameters describing the dissociation in the laboratory frame has also been introduced[20, 21]. Our theoretical work has, in part, been motivated by the beautiful experiments of Rakitzis *et al.* [14, 22, 23] who have measured the alignment of chlorine and bromine atoms resulting from the dissociation of HCl and HBr, respectively.

II. THEORY

The first step required in a theoretical investigation of photodissociation is to determine the underlying potential energy curves, the corresponding electronic transition dipole moments, and, if required, the non-adiabatic couplings between the electronic states. For HF and HCl, we have utilized PECs, dipole moments and spin-orbit couplings determined from *ab initio* calculations[2, 4]. For HI, both *ab initio* and empirical models for the electronic structure have been used[7–9].

Once the electronic structure is known, a methodology for treating the dynamics is required. In our work on the hydrogen halides[14–18] , a time-dependent wave packet treatment is utilized and the energy-dependent photofragmentation $\mathbf{T}$ matrix element associated with each channel n $\langle \Psi^-_{n,\Omega}(R,E)|\hat{\mathbf{d}}_q|\Psi_{\Omega_i}\rangle$, is determined. These are the critical quantities required for determining the $\mathbf{a}_Q^{(K)}(p)$ parameters via the dynamical functions $f_K(q,q')$ (see below). In order to determine the photofragmentation $\mathbf{T}$ matrix elements, the time-evolving wave packets are analyzed at each time step as they pass through an analysis line defined at a large fixed value of the bond length ($R = R_\infty$). By taking the Fourier transform over time of these cuts through the time-dependent wave packets, $\phi_n(R_\infty, t)$, energy dependent coefficients, $A_n(R_\infty, E)$, are obtained. The photofragmentation

T matrix elements are related to these energy dependent coefficients by[15]

$$\langle \Psi^-_{n,\Omega}(R,E)|\hat{\mathbf{d}}_q|\Psi_{\Omega_i}\rangle = i\left(\frac{h^2 k_v}{2\pi\mu}\right)^{\frac{1}{2}} e^{(-ik_v R_\infty)} A_n(R_\infty,E)$$
$$= i\left(\frac{h^2 k_v}{8\pi^3\mu}\right)^{\frac{1}{2}} e^{(-ik_v R_\infty)} \int_0^\infty \phi_n(R_\infty,t) e^{\frac{i}{\hbar}(E_i+h\nu)t} dt. \quad (1)$$

From the **T** matrix elements, the $\mathbf{a}_Q^{(K)}(p)$ parameters can be obtained via a well-established theoretical framework[19, 21, 24, 25]. The dimensionless anisotropy parameters, $\mathbf{a}_Q^{(K)}(p)$, are normalized combinations of the dynamical functions. For the dissociation of HX resulting in the production of a halogen atom and a hydrogen atom having angular momenta j_X and j_H, respectively, the dynamical functions for the halogen atom are related to the **T** matrix elements via

$$f_K(q,q') = \sum_{n,\Omega,\Omega_X,n',\Omega',\Omega'_X} (-1)^{K+j_X+\Omega'_X} \begin{pmatrix} j_X & j_X & K \\ -\Omega_X & \Omega'_X & q-q' \end{pmatrix}$$
$$\times (T^{n\Omega}_{j_X\Omega_X\, j_H\Omega_H})^* T^{n'\Omega'}_{j_X\Omega'_X\, j_H\Omega_H}$$
$$\langle \Psi^-_{n,\Omega}(R,E)|\hat{\mathbf{d}}_q|\Psi_{\Omega_i}\rangle^* \langle \Psi^-_{n',\Omega'}(R,E)|\hat{\mathbf{d}}_{q'}|\Psi_{\Omega_i}\rangle. \quad (2)$$

The indices q and q' are the vector spherical harmonic components [26] of the molecular electric dipole moment with respect to the recoil axis and can take the values 0 or ± 1 corresponding to parallel or perpendicular electronic transitions, respectively. The initial and final z-components of the total electronic angular momentum about the molecular axis are related by $\Omega = \Omega_i + q$. The diagonal ($q = q'$) and off-diagonal ($q \neq q'$) elements of the dynamical functions $f_K(q,q')$ correspond to incoherent and coherent excitation of different molecular continua.

Since the dynamical functions are directly related to the angular momentum state multipoles[15], K is referred to as the multipole rank. For the ground state halogen fragment X(^{2}P$_{3/2}$), the complete set of state multipoles (dynamical functions) contains $K = 0$ (population), $K = 1$ (orientation, dipole moment), $K = 2$ (alignment, quadrupole moment) and $K = 3$ (orientation, octupole moment). The description for the excited state halogen fragment X(^{2}P$_{1/2}$) requires only $K = 0$ and $K = 1$ dynamical functions. The relationships between the dynamical functions and the $\mathbf{a}_Q^{(K)}(p)$ parameters are described in Ref. [15] and two illustrative examples are given in Sec. III.

III. BRIEF SUMMARY OF RESULTS

In our studies of HF, HCl, and HI, the $\mathbf{a}_0^{(K)}(\perp)$ parameters ($K = 1-3$) describing incoherent perpendicular excitation and the $\mathbf{a}_2^{(K)}(\perp)$ parameters ($K = 2, 3$)

describing coherent perpendicular excitation have been computed for the ground state fragments $X(^2P_{3/2})$. For the excited state fragments $X(^2P_{1/2})$, the $\mathbf{a}_0^{(1)}(\perp)$ parameter and the $\mathbf{a}_1^{(1)}(\parallel,\perp)$ parameter, which describes coherent parallel and perpendicular excitation, have been computed.

For illustrative purposes, we only discuss one coherent and one incoherent parameter describing the production of ground state fragments. These parameters are related to the dynamical functions, Eq. 2, by

$$\mathbf{a}_0^{(2)}(\perp) = V_2(j_X)^{-1}\frac{f_2(1,1)}{f_0(1,1)} = \left[\frac{j_X(j_X+1)}{(2j_X+3)(2j_X-1)}\right]^{1/2}\frac{f_2(1,1)}{f_0(1,1)} \tag{3}$$

and

$$\mathbf{a}_2^{(2)}(\perp) = -\frac{1}{2}V_2(j_X)^{-1}\frac{f_2(1,-1)}{f_0(1,1)}. \tag{4}$$

The incoherent parameter $\mathbf{a}_0^{(2)}(\perp)$ is of interest because it can be related to the amount of $X(^2P_{3/2})$ produced via the $a^3\Pi_1$ state versus that from both $a^3\Pi_1$ and $A^1\Pi_1$, i.e.,

$$\mathbf{a}_0^{(2)}(\perp) = \frac{4(1-2p)}{5} \tag{5}$$

where $p = \sigma_{^3\Pi_1}/(\sigma_{^3\Pi_1}+\sigma_{^1\Pi_1})$. Clearly, this information can not be obtained by measurement of scalar parameters or β. For HF and HCl, this provides direct information on the non-adiabatic coupling from the $A^1\Pi_1$ state to the $a^3\Pi_1$ state since only the $A^1\Pi_1$ state is populated via direct excitation from the ground state. Figure 1 illustrates the $\mathbf{a}_0^{(2)}(\perp)$ anisotropy parameter describing incoherent perpendicular excitation for the ground state $X(^2P_{3/2})$ fragment produced from the photodissociation of $HX(v=0)$ as a function of photolysis wavelength. The coherent parameter $\mathbf{a}_2^{(2)}(\perp)$ is of interest because it can be related to the phase difference between the $a^3\Pi_1$ and $A^1\Pi_1$ states, i.e.,

$$\mathbf{a}_2^{(2)}(\perp) = \frac{-4\sqrt{2}}{5}\sqrt{(1-p)p}\,\cos(\phi^3\Pi_1 - \phi^1\Pi_1) \tag{6}$$

Figure 2 illustrates the $\mathbf{a}_2^{(2)}(\perp)$ anisotropy parameter describing incoherent perpendicular excitation for the ground state $X(^2P_{3/2})$ fragment produced from the photodissociation of $HX(v=0)$ as a function of photolysis wavelength.

For HF, HCl, and HI, the alignment and orientation of the halogen atoms resulting from photodissociation have been shown to be extremely sensitive to the details of the potential energy curves and transition dipole moments. More importantly, they provide more detailed information than measurement of the total cross-section, branching fraction, or the anisotropy parameter β alone.

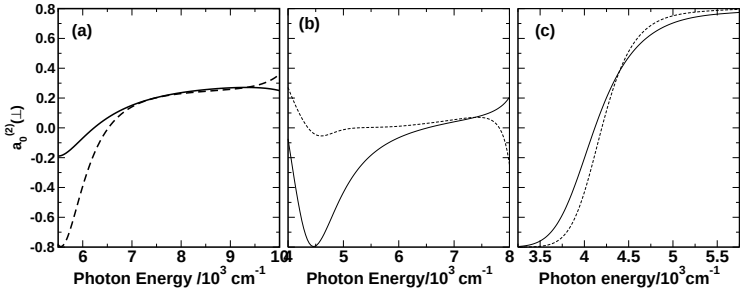

FIG. 1: Incoherent $\mathbf{a}_0^{(2)}(\perp)$ anisotropy parameter for the production of $X(^2P_{3/2})$ as a function of photon energy for the photodissociation of (a) HF/DF, (b) HCl/DCl, and (c) HI/DI. HX (solid line) and DX (dashed line).

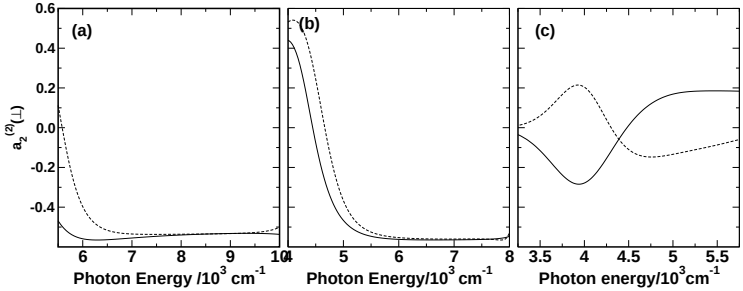

FIG. 2: Coherent $\mathbf{a}_2^{(2)}(\perp)$ anisotropy parameter for the production of $X(^2P_{3/2})$ as a function of photon energy for the photodissociation of (a) HF/DF, (b) HCl/DCl, and (c) HI/DI. HX (solid line) and DX (dashed line).

Acknowledgments. I thank the many people with whom I have had the privilege to collaborate with on various aspects of this work. My collaborators include G.G. Balint-Kurti, O.S. Vasyutinskii, T.P. Rakitzis, J.A. Beswick, A.J. Orr-Ewing and D.N. Jodoin. The financial support of the Natural Sciences and Engineering Research Council of Canada and the University of Alberta is gratefully acknowledged.

---

[1] J. Zhang, C. W. Riehn, M. Dulligan and C. Wittig, J. Chem. Phys. **104**, 7027 (1996).

[2] A. Brown and G. G. Balint-Kurti, J. Chem. Phys. **113**, 1870 (2001).
[3] P. M. Regan, D. Ascenzi, A. Brown, G. G. Balint-Kurti and A. J. Orr-Ewing, J. Chem. Phys. **112**, 10259 (2000).
[4] M. H. Alexander, B. Pouilly and T. Duhoo, J. Chem. Phys. **99**, 1752 (1993).
[5] P. M. Regan, S. R. Langford, A. J. Orr-Ewing and M. N. R. Ashfold, J. Chem. Phys. **110**, 281 (1999).
[6] B. Pouilly and M. Monnerville, Chem. Phys. **238**, 437 (1998).
[7] J. P. Camden, H. A. Bechtel, D. J. A. Brown, A. E. Pomerantz, R. N. Zare and R. J. LeRoy, J. Phys. Chem. A **108**, 7806 (2004).
[8] R. J. LeRoy, G. T. Kraemer and S. Manzhos, J. Chem. Phys. **117**, 9353 (2002).
[9] A. B. Alekseyev, H. P. Liebermann, D. B. Kokh and R. J. Buenker, J. Chem. Phys. **113**, 6174 (2000).
[10] P. M. Regan, D. Ascenzi, C. Clementi, M. N. R. Ashfold and A. J. Orr-Ewing, Chem. Phys. Lett. **315**, 187 (1999).
[11] S. R. Langford, P. M. Regan, A. J. Orr-Ewing and M. N. R. Ashfold, Chem. Phys. **231**, 245 (1998).
[12] D. J. Gendron and J. W. Hepburn, J. Chem. Phys. **109**, 7205 (1998).
[13] C. E. Moore, *Atomic Energy Levels* (U. S. Government Printing Office, Washington, DC, 1971).
[14] T. P. Rakitzis, P. C. Samartzis, R. L. Toomes, T. N. Kitsopoulos, A. Brown, G. G. Balint-Kurti, O. S. Vasyutinskii and J. A. Beswick, Science **300**, 1936 (2003).
[15] G. G. Balint-Kurti, A. J. Orr-Ewing, J. A. Beswick, A. Brown and O. S. Vasyutinskii, J. Chem. Phys. **116**, 10760 (2002).
[16] A. Brown, G. G. Balint-Kurti and O. S. Vasyutiniskii, J. Phys. Chem. A **108**, 7790 (2004).
[17] A. Brown, J. Chem. Phys. **122**, 084301 (2005).
[18] D. N. Jodoin and A. Brown, in press.
[19] T. P. Rakitzis and R. N. Zare, J. Chem. Phys. **110**, 3341 (1999).
[20] B. V. Picheyev, A. G. Smolin and O. S. Vasyutinskii, J. Phys. Chem. A **101**, 7614 (1997).
[21] E. R. Wouters, M. Ahmed, D. S. Peterska, A. S. Bracker, A. G. Suits and O. S. Vasyutinskii, in *Imaging in Chemical Dynamics*, ed. by A. G. Suits and R. E. Continetti (American Chemical Society, Washington, DC, 2000), p. 238.
[22] T. P. Rakitzis, P. C. Samartzis, R. L. Toomes, L. Tsigaridas, M. Coriou, D. Chestakov, A. T. J. B. Eppink, D. H. Parker and T. N. Kitsopoulos, Chem. Phys. Lett. **364**, 115 (2002).
[23] T. P. Rakitzis, P. C. Samartzis, R. L. Toomes and T. N. Kitsopoulos, J. Chem. Phys. **121**, 7222 (2004).
[24] L. D. A. Siebbeles, M. Glass-Maujean, O. S Vasyutinskii, J. A. Beswick and O. Roncero, J. Chem. Phys. **100**, 3610 (1994).
[25] A. S. Bracker, E. R. Wouters, A. G. Suits and O. S. Vasyutinskii, J. Chem. Phys. **110** 6749 (1999).
[26] R. N. Zare, *Angular Momentum* (World Scientific, New York, 1988).